https://doi.org/10.5194/egusphere-2026-858
Preprint. Discussion started: 2 April 2026

Conditioning-controlled retrieval of broadband land surface temperature and emissivity from paired ground-based longwave irradiance measurements

Collins Mito

Department of Physics, Faculty of Science and Technology, University of Nairobi, Nairobi, P.O. Box 30197-00100, Kenya

Correspondence to: Collins Mito (collins@uonbi.ac.ke)

Abstract. Accurate retrieval of land surface temperature (LST) from broadband longwave radiometric measurements is fundamentally limited by the nonlinear coupling between surface emissivity and temperature, which can render the inverse problem weakly observable under low irradiance contrast. We present a conditioning-controlled retrieval methodology that estimates broadband surface emissivity and LST directly from paired ground-based upwelling and downwelling longwave irradiance measurements acquired at high temporal resolution. The approach combines adaptive temporal pairing constrained by a quasi-steady apparent surface temperature criterion with a fixed-iteration Newton inversion, and explicitly diagnoses inversion stability through Jacobian strength, residual magnitude, and observed convergence order. A formal uncertainty propagation framework is developed for both independent and correlated irradiance error structures, enabling decomposition of irradiance-driven and emissivity-driven temperature uncertainty. The method is evaluated using 39 datasets from four Surface Radiation Budget (SURFRAD) Network sites spanning diverse atmospheric conditions. The Newton inversion exhibited stable and well-conditioned behaviour across all cases, and retrieved surface temperatures agreed with independent in-situ measurements with a root mean square error of 0.54 K and a mean absolute error of 0.47 K, consistent with propagated uncertainty estimates. Results demonstrate that reliable broadband LST retrieval can be achieved without externally prescribed emissivity products when inversion conditioning and measurement uncertainty are explicitly incorporated into the retrieval design.

1 Introduction

Land surface temperature (LST) is a fundamental variable in studies of surface energy balance, land-atmosphere coupling, hydrology, and climate variability (Li et al., 2013; Wan et al., 2015). Accurate estimation of LST is essential for understanding surface fluxes, diagnosing land-atmosphere feedbacks, and evaluating satellite-based thermal infrared products. While satellite observations provide global coverage, ground-based radiometric networks remain indispensable for algorithmic development, physical interpretation, and validation.

Broadband longwave irradiance measurements offer a direct link between surface state and observed radiation, but converting these to temperature is non-trivial due to emissivity coupling. Most existing approaches for deriving surface temperature from

https://doi.org/10.5194/egusphere-2026-858
Preprint. Discussion started: 2 April 2026

SURFRAD observations prescribe surface emissivity externally, typically using satellite-derived narrowband emissivity products from sensors such as MODIS (Zhang et al (2016); Wang et al (2019); Li et.al (2014)). These emissivities are often obtained from coarse resolution, temporally composited products and then converted into broadband values. While widely used, this practice introduces multiple sources of uncertainty, including spatial mismatch between instantaneous in situ observations and multi-day composites, temporal mismatch, and spectral mismatch between narrowband emissivities and broadband irradiance exchange (Gillespie et al., 1998; Hulley and Hook, 2011; Li et al., 2019). In addition, emissivity uncertainty is rarely propagated explicitly, and the numerical conditioning of the resulting surface temperature estimate is seldom examined.

From an inverse-problem perspective, the challenge is more fundamental. Broadband upwelling irradiance depends jointly on surface temperature, surface emissivity, and downwelling atmospheric irradiance. With a single observation, emissivity and temperature are inseparable even with multiple observations, the problem may remain ill-conditioned if the observations are poorly chosen. As a result, emissivity retrieval can become numerically unstable, leading to amplified uncertainty in surface temperature estimates. Despite this, many previous studies focus primarily on retrieval accuracy while giving limited attention to convergence behavior, conditioning, and uncertainty structure.

The high temporal resolution of SURFRAD measurements provides an opportunity to address this limitation. Ground-based broadband longwave radiometric networks such as SURFRAD provide continuous, well calibrated measurements of upwelling and downwelling longwave radiation (Augustine et al., 2000; Augustine et al., 2005). Over short time intervals, surface emissivity may be treated as invariant, while surface temperature can be assumed to vary slowly. Temporal pairing of irradiance measurements therefore introduces additional information that improves emissivity observability without altering the underlying physics. However, temporal paring alone does not guarantee a well posed inversion. Explicit attention to numerical conditioning, convergence diagnostics, and uncertainty propagation is required to ensure physically meaningful and stable solutions.

In this study, a diagnostic-driven framework for retrieving broadband surface emissivity and surface temperature directly from paired upwelling and downwelling longwave irradiance measurements is presented. The method employs adaptive temporal pairing constrained by quasi-steady apparent surface temperature, followed by a fixed-iteration Newton inversion of emissivity. Rather than relying solely on retrieval accuracy, the approach emphasizes convergence diagnostics, Jacobian conditioning, and uncertainty decomposition. A linearized emissivity estimate is used strictly as a diagnostic tool, while the Newton solution is retained as the physically meaningful estimate. Surface temperature uncertainty is explicitly decomposed into irradiance-driven and emissivity-driven components, enabling transparent interpretation of retrieval reliability.

The remainder of the paper is organized as follows. Section 2 introduces the physical and conceptual background underlying broadband longwave irradiance coupling, apparent surface temperature, and emissivity observability. Section 3 presents the emissivity inversion methodology, including the irradiance model, adaptive temporal pairing, Newton inversion, convergence diagnostics, sensitivity analysis, and uncertainty propagation. Section 4 describes the experimental setup and validation framework, including data coverage, reference emissivity and temperature sources, and contextual comparison with existing

https://doi.org/10.5194/egusphere-2026-858
Preprint. Discussion started: 2 April 2026

SURFRAD-based approaches. Section 5 presents the results, focusing on numerical convergence behavior, conditioning diagnostics, emissivity retrieval performance, surface temperature validation, and uncertainty decomposition. Finally, Sect. 6 summarizes the main findings and discusses the implications of the proposed diagnostics-driven framework for broadband surface temperature retrieval from ground-based radiometric observations.

2 Physical and conceptual background

Broadband longwave irradiance exchange between the surface and atmosphere is governed by surface emissivity, surface temperature, and atmospheric emission (Rodgers, 2000; Li et al., 2013). At the land-atmosphere interface, the upwelling longwave irradiance measured above the surface represents the combined contribution of surface emission and reflected downwelling atmospheric irradiance, while the downwelling component captures atmospheric emission incident on the surface. In broadband form, these quantities are commonly expressed through the Stefan-Boltzmann framework, in which surface emissivity and surface (skin) temperature jointly govern the emitted irradiance flux. However, land surface temperature retrieval remains fundamentally limited by emissivity observability and irradiance coupling (Li et al., 2023; Dash et al., 2002). A fundamental challenge arises because broadband irradiance measurements alone do not uniquely constrain both surface emissivity and surface temperature. For a single observation, the two quantities are nonlinearly coupled, leading to an underdetermined and potentially ill-conditioned inverse problem. Small perturbations in emissivity can induce disproportionately large changes in retrieved temperature, particularly under conditions of high emissivity or strong atmospheric downwelling irradiance. This coupling has motivated many previous studies to rely on externally prescribed emissivity values, often derived from satellite products, when converting in situ broadband irradiance to land surface temperature.

An alternative perspective is provided by the concept of apparent surface temperature, defined directly from the measured upwelling irradiance under the assumption of unit emissivity. Although this apparent temperature does not represent the true physical surface temperature (Norman et al., 1995; Li et al., 2013), it is fully observable from irradiance measurements and provides a physical meaningful upper bound on the actual surface temperature. Importantly, variations in apparent temperature over short intervals primarily reflect changes in radiative forcing rather than abrupt changes in surface thermodynamic state.

High temporal resolution broadband longwave observations offer an opportunity to exploit this property. Over sufficiently short time windows (60 seconds for SURFRAD), surface emissivity can be assumed invariant and the true surface temperature quasi-steady, while atmospheric irradiance conditions evolve enough to introduce measurable contrast in upwelling and downwelling irradiance. Temporal pairing of broadband irradiance measurements therefore introduces additional physical information that improves emissivity observability without modifying the underlying irradiance physics.

However, the use of temporal information alone does not guarantee a well-posed inversion. Poorly chosen temporal pairs can amplify temperature variability or lead to weak irradiance contrast, resulting in numerical instability and unreliable emissivity

https://doi.org/10.5194/egusphere-2026-858
Preprint. Discussion started: 2 April 2026

estimates. Any physically meaningful retrieval strategy must therefore incorporate explicit constraints that preserve quasi-steady surface conditions while enhancing irradiance contrast, and must assess the conditioning of the resulting inversion. In this study, these principles motivate a diagnostic-driven emissivity and surface temperature retrieval framework that relies solely on paired broadband upwelling and downwelling irradiance measurements. The following section formalizes this framework through a nonlinear inversion scheme with explicit convergence diagnostics, sensitivity analysis, and uncertainty propagation, ensuring that numerical stability and physical interpretability are treated as integral components of the retrieval rather than post-hoc considerations.

3 Emissivity and surface temperature retrieval

This section describes the irradiance formulation, emissivity inversion strategy, numerical diagnostics, and uncertainty propagation framework used to retrieve broadband surface emissivity and land surface temperature from paired upwelling and downwelling longwave irradiance measurements. The methodology is intentionally diagnostic-driven, emphasizing conditioning, convergence behavior, and uncertainty control rather than accuracy alone.

3.1 Irradiance model

Surface thermal emission is modelled using a two-component broadband longwave irradiance balance that accounts explicitly for surface emissivity and atmospheric downwelling irradiance. Assuming that sensor measures hemispherically integrated longwave irradiance, the upwelling longwave irradiance measured above the surface at a given time is expressed as:

$$L = \varepsilon\sigma T_s^4 + (1-\varepsilon)\, l\,, \tag{1}$$

where: L is the measured upwelling longwave irradiance (Wm^{-2}); σ is the Stefan-Boltzmann constant ($\approx 5.67\text{x}10^{-8} Wm^{-2}K^{-4}$); T_s is the absolute surface temperature (K); l is the downwelling atmospheric longwave irradiance (Wm^{-2}), and ε is the broadband surface emissivity. Equation (1) assumes hemispherical emission and reflection and is appropriate for broadband longwave irradiance exchange at the surface. Rearranging Eq. (1) yields $\varepsilon(\sigma T_s^4 - l) = L - l$ which highlights that emissivity and surface temperature are intrinsically coupled through the emitted term.

To find the surface temperature from the other known measured quantities, we algebraically isolate T_s in Eq. (1) to get emissivity-corrected surface temperature:

$$T_s = \left(\frac{L-(1-\varepsilon)l}{\varepsilon\sigma} \right)^{1/4}, \tag{2}$$

Equation (2) is widely used in surface energy balance studies when emissivity is prescribed. However, when emissivity is unknown, Eq. (2) highlights the strong nonlinear coupling between emissivity and temperature. An apparent (emissivity-independent) surface temperature is also defined directly from the measured upwelling irradiance:

https://doi.org/10.5194/egusphere-2026-858
Preprint. Discussion started: 2 April 2026

$$T_s^{'} = \left(\frac{L}{\sigma}\right)^{1/4} \tag{3}$$

Although $T_s^{'}$ does not represent the true surface temperature, it provides a physically meaningful upper bound and is fully observable from irradiance measurements. The difference between this apparent temperature and the true surface temperature reflects emissivity effects. This quantity is later used as a constraint in adaptive temporal pairing.

Equation (2) illustrates three important implications. First, emissivity and temperature are inseparable from a single broadband observation, rendering the inverse problem undetermined. Second, small emissivity errors can lead to large temperature errors, particularly near $\varepsilon \to 1$. Third, at viewing altitudes above the surface, additional atmospheric terms would further complicate the relationship. In this study, the initial focus is rigorously maintained on surface ground-based broadband irradiance measurements where atmospheric transmittance effects are negligible. This choice is intentional, as it isolates the fundamental ill-conditioning caused solely by the nonlinear $\varepsilon - T_s$ coupling. The diagnostic framework developed is, however, structurally extensible to these more complex radiative transfer scenarios, as discussed in Sect. 6.

3.2 Newton inversion

This section describes the formulation of the Newton inversion, the initialization strategy, and the numerical behavior of the iterative solution. Emphasis is placed on ensuring physical consistency, numerical stability, and diagnostic transparency rather than on enforcing convergence through arbitrary stopping criteria. The subsections that follow detail the construction of the nonlinear objective function, the treatment of emissivity-temperature coupling, and the diagnostics used to assess convergence, conditioning and solution reliability.

3.2.1 Broadband emissivity retrieval

Broadband emissivity is retrieved by solving an implicit nonlinear equation derived from the two time irradiance model. Equation (2) can be written in a more convenient form by introducing the emissivity-induced temperature correction ΔT :

$$T_s = T_s^{'} - \Delta T\,, \tag{4}$$

where:

$$\Delta T = \frac{1}{\sigma^{1/4}}\left[L^{1/4} - \left(\frac{L-(1-\varepsilon)l}{\varepsilon}\right)^{1/4}\right], \tag{5}$$

The emissivity-induced temperature correction ΔT is defined as the difference between the apparent (blackbody) surface temperature $T_s^{'}$ and the emissivity-corrected surface temperature T_s. Expressed directly in terms of measured upwelling and downwelling irradiances, ΔT is given by Eq. (5). This formulation ensures dimensional consistency, vanishes in the blackbody limit ($\varepsilon = 1$), and is fully consistent with the numerical implementation. Rearranging Eq. (5) yields:

https://doi.org/10.5194/egusphere-2026-858
Preprint. Discussion started: 2 April 2026

$$\varepsilon = \frac{L - l}{(L^{1/4} - \sigma^{1/4}\Delta T)^{4} - l} \tag{6}$$

To reduce sensitivity to absolute calibration errors and slowly varying atmospheric conditions, the inversion uses two irradiance measurements (t_1, t_2) acquired within a short interval ($dt \le 60\ s$) where emissivity is assumed invariant.

Henceforth, upwelling irradiance at time t_i is denoted L_i , and downwelling irradiance as l_i to simplify the two-time notation. The emissivity-induced temperature correction is then approximated as:

$$\Delta T \approx \overline{\Delta T} = \frac{1}{2}\left(\Delta T_1 + \Delta T_2\right), \tag{7}$$

where:

$$\Delta T_i = \frac{1}{\sigma^{1/4}}\left[L_i^{1/4} - \left(\frac{L_i - l_i}{\varepsilon} + l_i\right)^{1/4}\right],\ i = 1, 2$$

Substituting this approximation into Eq. (6) yields an implicit nonlinear equation in emissivity:

$$f(\varepsilon) = \varepsilon\left[\left(P_1 - M(\varepsilon)\right)^4 - l_1\right] - N\ , \tag{8}$$

where:

$$M(\varepsilon) = \frac{1}{2}\left[(P_1) + (P_2) - \left(\frac{L_1 - l_1}{\varepsilon} + l_1\right)^{1/4} - \left(\frac{L_2 - l_2}{\varepsilon} + l_2\right)^{1/4}\right]$$

$$N = L_1 - l_1$$

$$P_i = (L_i)^{1/4}$$

Equation (8) contains emissivity both explicitly and implicitly through ΔT , and therefore must be solved numerically. The root is obtained using the-Newton-Raphson method (Ortega and Rheinboldt, 2000; Nocedal and Wright, 2006):

$$\varepsilon_{k+1} = \varepsilon_k - \frac{f(\varepsilon_k)}{f'(\varepsilon_k)}\ , \tag{9}$$

where: $k = 0, 1, 2.....(n-1)$ is the iteration index, and n is the number of iterations. The derivative of Eq. (8), $f'(\varepsilon)$ is computed analytically using the chain and product rules to get:

$$f'(\varepsilon) = \left[\left(P_1 - M(\varepsilon)\right)^4 - l_1\right] + \varepsilon\left[-4\left(P_1 - M(\varepsilon)\right)^3 M'(\varepsilon)\right], \tag{10}$$

where:

$$M'(\varepsilon) = -\frac{1}{8}\left[\left(\frac{L_1 - l_1}{\varepsilon} + l_1\right)^{-3/4}\frac{L_1 - l_1}{\varepsilon^2} + \left(\frac{L_2 - l_2}{\varepsilon} + l_2\right)^{-3/4}\frac{L_2 - l_2}{\varepsilon^2}\right]$$

https://doi.org/10.5194/egusphere-2026-858
Preprint. Discussion started: 2 April 2026

For this diagnostic analysis, a fixed, small maximum number of iterations, $N_{Newton} \leq 8$ is used instead of a dynamic convergence tolerance. This deliberate choice allows for transparent, post-hoc analysis of the convergence rate (p_k), residual magnitude, and Jacobian strength across every case, which is central to diagnosing solution stability (Sect. 3.3). Solutions are constrained to the physically meaningful range $0 < \varepsilon < 1$. This fixed iteration count, N_{Newton}, should be distinguished from the adaptive temporal adjustment count, N_{adj}, reported in Table 1 and Figure 4, which reflects data selection effort. It should be noted that for an operational implementation, a dynamic stopping criterion would be employed, as discussed in Sect. 6.

3.2.2 Determination of the initial (linearized) emissivity estimate

The convergence and stability of the Newton-Raphson method are inherently sensitive to the choice of the initial guess ε_0. For the nonlinear irradiance balance defined in Eq. (8), a robust initialization strategy ensures the iteration begins within the basin of attraction of the physical root. While it is assumed that only one physical meaningful root exists within the domain $0 < \varepsilon < 1$, a robust initialization strategy is required to ensure the iteration begins within the basin of attraction of this root.
A physically motivated initial guess is derived via a first-order Taylor expansion of the fourth-root terms:

$$\left(\frac{L_i - l_i}{\varepsilon} + l_i\right)^{1/4} \approx (l_i)^{1/4} + \frac{1}{4}(l_i)^{-3/4}\left(\frac{L_i - l_i}{\varepsilon}\right), \tag{11}$$

Substituting this linear approximation in the governing equation, Eq. (8), allows for the algebraic isolation of emissivity. By applying a binomial expansion and truncating at the first-order term, we obtain the linearized emissivity estimate:

$$\varepsilon_0 \approx \frac{N - Q}{P} = \frac{(L_1 - l_1) - 4MJ^3}{J^4 - l_1} \tag{12}$$

The quantities N, M, J, P and Q are algebraic combinations of the measured upwelling (L_i) and downwelling (l_i) irradiances. Specifically, $N = L_1 - l_1$ represents the net surface-emitted irradiance at the first time step; the coefficient M arises from a first-order Taylor expansion of the fourth-root temperature correction with respect to emissivity and is defined as $M = \frac{1}{8}\sum_{i=1}^{2}\left(L_i - l_i\right)l_i^{-3/4}\Big)$; the term J represents an effective irradiance contrast between upwelling and downwelling fields and is given by $J = \frac{1}{2}\sum_{i=1}^{2}\left((-1)^{i-1}L_i^{1/4} + l_i^{1/4}\right)$; the quantity Q is $Q = 4MJ^3$; and $P = J^4 - l_1$.

The linearized emissivity provides a physically motivated initial guess for Newton's method. Importantly, ε_0 is retained strictly as a diagnostic and initialization aid. Its value provides a crucial baseline: it represents the solution obtainable if the system were purely linear or if the non-linear coupling terms were ignored. As demonstrated in Sect. 3.5.1, its uncertainty diverges dramatically under conditions of weak irradiance contrast where the linearization assumption breaks down. This

https://doi.org/10.5194/egusphere-2026-858
Preprint. Discussion started: 2 April 2026

divergence, rather than the magnitude of ε_0 itself, serves as a critical diagnostic confirming the necessity of the full Newton inversion and its associated Jacobian control.

3.2.3 Corrected surface temperature, T_s retrieval

Once the broadband emissivity ε is retrieved via the Newton-Raphson method, the final corrected surface temperature T_s is computed by applying the correction term ΔT to the mean apparent surface temperature. In this framework, the mean apparent (blackbody) surface temperature $T_s^{'}$ is derived from the upwelling irradiances at the two observation times:

$$T_s^{'} = \frac{1}{2\sigma^{1/4}}\left[(L_1)^{1/4} + (L_2)^{1/4}\right] \tag{13}$$

This mean apparent temperature serves as the observable baseline for the retrieval. The final physically corrected surface temperature is then obtained by subtracting the emissivity-induced correction term from this baseline: $T_s = T_s^{'} - \Delta T$. By using the mean of the two irradiance measurements, the retrieval becomes less sensitive to instantaneous instrument noise and transient micro-scale fluctuations.

To ensure the validity of the two-time irradiance model, candidate irradiance pairs must satisfy the quasi-steady apparent temperature constraint:

$$\left|T_s^{'}(t_2) - T_s^{'}(t_1)\right| \le \Delta T_{\max}^{'} \tag{14}$$

This constraint serves a critical dual purpose in the diagnostic framework. First, it enforces physical consistency. The retrieval assumes that the surface emissivity is invariant and the true skin temperature T_s varies slowly over the interval Δt . By limiting the change in apparent (blackbody) temperature to a small threshold (e.g., $\Delta T_{\max}^{'} \approx 1\,K$), the algorithm filters out periods of rapid thermal transition, such as those caused by cloud shadows, sudden wind gusts, or the onset of precipitation. Second, it optimizes numerical conditioning. If the change in apparent temperature is too large, the $\varepsilon - T_s$ coupling in the Newton Jacobian becomes non-stationary, leading to emissivity-driven temperature errors. By enforcing Eq. (14), the algorithm ensures that the observed irradiance differences are primarily driven by the contrast between surface emission and atmospheric downwelling irradiance rather than shifting thermodynamic state. This makes Eq. (14) a fundamental diagnostic filter that precedes the inversion, ensuring that only well-posed data pairs are passed to the Newton solver.

3.3 Newton diagnostics for emissivity inversion

Because convergence of a nonlinear solver does not, by itself, guarantee physical observability or numerical reliability, the emissivity inversion is evaluated using a set of complementary Newton diagnostics. These diagnostics quantify irradiance consistency, local curvature of the inversion, and convergence behavior, allowing well-conditioned solutions to be distinguished from cases where convergence occurs under weak emissivity observability. The following subsections describe

https://doi.org/10.5194/egusphere-2026-858
Preprint. Discussion started: 2 April 2026

the residual magnitude, Jacobian strength, observed order of convergence, and iteration count diagnostics, and explain how they are interpreted collectively to assess the stability and physical reliability of the retrieved emissivity.

3.3.1 Residual magnitude

At the final Newton iteration, the residual magnitude $|f(\varepsilon)|$, defined in Eq. (8), quantifies the degree to which the irradiance balance equation is satisfied by the retrieved emissivity (Tarantola, 2005; Rodgers, 2000). This diagnostic is independent of convergence rate and provides a direct measure of self-consistency between the solution and the observed upwelling and downwelling irradiance measurements. A small residual indicates that the retrieved emissivity produces the measured irradiances within the limits of the forwarded model.

The residual threshold adopted in this study given by Eq. (15), is selected to be consistent with the expected magnitude of irradiance measurement uncertainty:

$$Residual\quad flag = \begin{cases} Excellent\quad radiative\quad consistency & r \le 10^{-3} \\ Acceptable (radiance\quad noise\quad limited) & 10^{-3} < r \le 10^{-2} \\ Poor\quad fit (likekly\quad ill-conditioned) & r > 10^{-2} \end{cases}, \tag{15}$$

Reducing the residual below this level would imply fitting noise rather than physically meaningful signal and is therefore not pursued. The residual magnitude thus serves as a necessary condition for a physically admissible solution, ensuring that the inversion does not violate irradiance balance. However, a small residual does not guarantee that the emissivity is well constrained. In particular, Newton's method may converge to a solution with a small residual in regions where the forward model is weakly sensitive to emissivity, leading to large uncertainty despite apparent convergence. For this reason, residual-based diagnostics must be interpreted in conjunction with Jacobian-based conditioning metrics, which are discussed in the following subsection.

3.3.2 Jacobian strength

The minimum Jacobian magnitude, denoted $\min|\partial f / \partial \varepsilon|$, is defined as the smallest absolute value of the Newton Jacobian encountered during the inversion. This quantity characterizes the local curvature of the nonlinear irradiance balance equation with respect to emissivity and directly controls the stability and uncertainty of the retrieved solution. From implicit differentiation of the governing equation we get:

$$\frac{\partial \varepsilon}{\partial L} \propto \left(\frac{\partial f}{\partial \varepsilon}\right)^{-1}, \tag{16}$$

indicating that small Jacobian magnitudes lead to large amplification of measurement uncertainty in the retrieved emissivity. Physically, a small Jacobian corresponds to a locally flat inversion surface, (Tarantola, 2005; Menke, 2012; Aster et al., 2019), implying weak sensitivity of the irradiance model to emissivity and, poor observability. The first-order uncertainty relationship

https://doi.org/10.5194/egusphere-2026-858
Preprint. Discussion started: 2 April 2026

expressed in Eq. (16) is mathematically exact under linearization and forms the basis for interpreting Jacobian strength as a conditioning diagnostic. Thresholds used to classify Jacobian behavior, given in Eq. (17) are not universal constants but are instead selected relative to the observed growth of emissivity uncertainty:

$$Jacobian\quad flag=\begin{cases} Strong\quad emissivity\quad observability & J_{\min}>10^{3} \\ Moderate\quad observability & 10^{2}<J_{\min}\le 10^{3} \\ Weak/ill-conditioned & J_{\min}\le 10^{2} \end{cases} \tag{17}$$

This approach ensures that conditioning is assessed in a data-consistent and physically meaningful manner. Accordingly, Jacobian strength is interpreted in conjunction with uncertainty behavior rather than in isolation. This data-driven classification avoids arbitrary numerical cutoffs and provides a robust indicator of whether the emissivity retrieval is well constrained by the available irradiance information.

3.3.3 Observed order of convergence

The observed order of convergence provides a local, data-driven measure of how the Newton iteration behaves near solution (Ortega and Rheinboldt, 2000; Dennis and Schnabel, 1996). If the iteration-to-iteration change in emissivity be defined as: $\Delta_k=\left|\varepsilon_{k+1}-\varepsilon_k\right|$. The observed convergence order is then estimated as:

$$p_k=\frac{\log(\Delta_k/\Delta_{k-1})}{\log(\Delta_{k-1}/\Delta_{k-2})} \tag{18}$$

This quantity characterizes the local curvature of the objective function and is independent of the residual magnitude. As such, it provides complementary diagnostic information to residual and Jacobian based measures. In particular, the observed order of convergence reveals whether Newton's method is operating in a regime consistent with theoretical expectations or whether convergence is limited by weak curvature, noise or ill-conditioning.

This diagnostic is especially important for interpreting uncertainty behavior. Case exhibiting near-linear convergence ($p_k\approx 1$) indicate reduced curvature and increased sensitivity to measurement noise, while values approaching quadratic convergence reflect well-conditioned local behavior. Conversely, sub-linear convergence signals poor observability and limited physical interpretability of the retrieved emissivity. Based on these considerations, Eq. (19) defines diagnostic thresholds used to classify convergence behavior:

$$Convergence\quad flag=\begin{cases} Quadratic\quad convergence\quad (well\quad posed) & 1.7\le p_k\le 2.3 \\ Linear\quad convergence & 0.8\le p_k\le 1.7 \\ Flat/ill-conditioned & p_k<0.8 \\ Overshoot/numerical\quad instability & p_k>2.3 \end{cases} \tag{19}$$

https://doi.org/10.5194/egusphere-2026-858
Preprint. Discussion started: 2 April 2026

These classifications follow directly from Newton convergence theory and are independent of the specific radiative transfer application, making the observed convergence order a robust and general indicator of numerical reliability.

3.3.4 Number of Newton iterations

The number of Newton iterations required for convergence provides useful but limited diagnostics information when considered in isolation. Iteration count does not, by itself, indicate whether convergence is physically meaningful or numerically well-conditioned. A small number of iterations may occur in both strongly and weakly constrained problems, while a larger number of iterations does not necessarily imply instability.

For this reason, iteration count is interpreted jointly with Jacobian strength and the observed order convergence. Together, these diagnostics distinguish rapid convergence driven by strong local curvature from apparent convergence occurring in flat or weakly sensitive regions of the objective function. The iteration based diagnostic flag defined in Eq. (20) reflects this combined interpretation rather than treating iteration count as a standalone measure of performance:

$$Iteration \quad flag = \begin{cases} Strong \quad curvature & N_{Newton} \le 5 \\ Moderate \quad conditioning & 6 \le N_{Newton} \le 8 \\ Weak \quad curvature/\ flat \quad Jacobian & N_{Newton} > 8 \end{cases} \tag{20}$$

In the present framework, iteration count is therefore used as a supporting indicator of numerical behavior, complementing residual, Jacobian, and observed order of convergence diagnostics to provide a complete assessment of inversion stability and conditioning.

3.3.5 Combined diagnostic logic

Newton convergence in this study is evaluated using a complementary set of diagnostics: residual magnitude, Jacobian strength, observed order of convergence, and iteration count. Together, these measures assess irradiance self-consistency, emissivity observability, and numerical conditioning of the inversion. Each diagnostic targets a distinct failure mode and cannot, on its own, guarantee physical reliability.

Solutions exhibiting small residuals but weak Jacobian strength or sub-linear convergence behavior are identified as ill conditioned and are consistently associated with inflated emissivity uncertainty. Such cases indicate convergence driven by flat or weakly sensitive regions of the objective function rather than by robust physical information. The combined diagnostic logic therefore distinguishes between convergence that reflects genuine emissivity observability and convergence that occurs despite poor conditioning.

Based on the diagnostic flag scheme defined above, a solution is considered physically reliable when the combined criteria in Eq. (21) are satisfied. These criteria provide data-driven bounds that distinguish well-conditioned from weakly conditioned inversions within the context of SURFRAD instrumentation noise levels. The diagnostics are used to interpret solution reliability and uncertainty behavior, rather than to enforce hard rejection of results:

https://doi.org/10.5194/egusphere-2026-858
Preprint. Discussion started: 2 April 2026

$$\begin{aligned} &|f(\varepsilon)| \le 10^{-3} \\ &J_{\min} > 10^{2} \\ &p_k \ge 1 \\ &N_{iter} \le 8 \end{aligned} \tag{21}$$

Although the form and interpretation of these diagnostics are well established in inverse-problem and numerical-analysis frameworks, their numerical thresholds depend on problem scaling and measurement uncertainty. In this study, thresholds were selected based on observed transitions in emissivity uncertainty growth and Newton convergence behavior, ensuring consistency with the data characteristics and the underlying irradiance physics.

3.4 Sensitivity analysis

To understand how irradiance measurements, emissivity, and surface temperature interact with the inversion, a formal sensitivity and uncertainty analysis is performed. Sensitivity analysis quantifies how small perturbations in the measured irradiances propagate through the retrieval, revealing the mechanisms that control emissivity and temperature observability. Uncertainty propagation then translates instrument-level irradiance uncertainty into physically interpretable uncertainty bounds on the retrieved emissivity and surface temperature. Together, these analyses clarify the conditioning of the inversion, explain diagnostic behavior, and provide the theoretical basis for the uncertainty estimates reported in the results section.

This section examines how perturbations in broadband upwelling and downwelling longwave irradiance measurements influence (i) the linearized emissivity, (ii) the Newton-retrieved emissivity, and (iii) the corrected surface temperature. The objective is to identify dominant sensitivity pathways and physical regimes, independent of numerical convergence.

3.4.1 Sensitivity of the initial (linearized) emissivity estimate

The sensitivity of the linearized emissivity estimate ε_0 is examined by performing a total differentiation of its governing algebraic expression derived in Sect. 3.2.2. This analysis identifies the physical and numerical pathways through which small fluctuations in measured longwave irradiance propagate into the initial estimate. Applying the total differential to Eq. (12) yields:

$$\delta\varepsilon_0 = \frac{1}{P}\left(\delta N - \delta Q\right) - \frac{N-Q}{P^2}\delta P \tag{22}$$

This expression reveals three distinct sensitivity pathways that characterize the behavior of the linearized estimate:

1. The term $\delta N / P$ represents sensitivity arising directly from perturbations in the irradiance contrast at the first time step. This contribution increases as surface-emitted irradiance decreases. Under humid conditions, where atmospheric downwelling irradiance can approach the upwelling component, this sensitivity is amplified. This pathway is local to first measurement time and is independent of the second irradiance observation;

https://doi.org/10.5194/egusphere-2026-858
Preprint. Discussion started: 2 April 2026

2. The term $\delta Q / P$ depends on both measurement times through the quantities M and J. Sensitivity increases when the temporal irradiance contrast is weak, i.e., when J is small. This pathway explicitly couples emissivity to surface temperature variability, such that even small irradiance perturbations at either time can propagate strongly when temporal contrast is limited;
3. The final term, proportional to $\delta P / P^2$, represents sensitivity associated with the conditioning of the denominator. Since $P = J^4 - l_1$, small values of J or large atmospheric contributions l_1 can drive P toward zero. Under typical observational conditions, characterized by humid atmospheres and weak short-term irradiance contrast, this pathway dominates and can lead to extreme sensitivity amplification.

The key implication of this analysis is that the linearized emissivity estimate is structurally sensitive under standard observational conditions. Although it may yield emissivity values close to Newton solution, its sensitivity behavior is dominated by conditioning effects rather than physical robustness. Consequently, the linearized emissivity should be interpreted strictly as a diagnostic initialization and not as a physical reliable emissivity estimate.

3.4.2 Sensitivity of Newton-retrieved emissivity

The emissivity ε is obtained by solving the implicit nonlinear equation:

$$f(\varepsilon; L) = 0, \tag{23}$$

where $L = \{L_1, l_1, L_2, l_2\}$ denotes the measured upwelling and downwelling longwave irradiances. Because the solution satisfies $f(\varepsilon; L) = 0$, application of the implicit function theorem yields the total differential:

$$\frac{\partial f}{\partial \varepsilon}\delta\varepsilon + \sum_i \frac{\partial f}{\partial L_i}\delta L_i = 0 \tag{24}$$

This gives the emissivity sensitivity to irradiance perturbations as:

$$\delta\varepsilon = -\frac{1}{\partial f / \partial \varepsilon}\sum_i \frac{\partial f}{\partial L_i}\delta L_i \tag{25}$$

Here, $\partial f / \partial \varepsilon$ is the Jacobian of the inversion. Eq. (25) shows that all emissivity sensitivity is controlled by the Jacobian magnitude. When the Jacobian is small, emissivity becomes weakly observable, regardless of how small the irradiance measurement noise may be.

From Eq. (10), the Jacobian can be decomposed into two physically distinct components. The first term represents the irradiance curvature term J_{irrad}:

$$J_{irrad} = (P_1 - M(\varepsilon))^4 - l_1 \tag{26}$$

This term represents irradiance contrast $L - l(1-\varepsilon)$; it is maximized under dry conditions and diminishes under humid or cloudy skies.

https://doi.org/10.5194/egusphere-2026-858
Preprint. Discussion started: 2 April 2026

The second contribution is the emissivity-temperature coupling term:

$$J_{\varepsilon T} = \varepsilon\left(-4\left(P_1 - M(\varepsilon)\right)^3 M'(\varepsilon)\right) \tag{27}$$

This term arises because changes in emissivity modify the retrieved surface temperature, which then feeds back into the irradiance balance. Its sensitivity increases as emissivity approaches unity and as irradiance contrast weakens. When dominant, this coupling introduces nonlinearity and further reduces Jacobian strength rendering emissivity weakly observable.

The full Jacobian structure may therefore be written as:

$$\frac{\partial f}{\partial \varepsilon} = J_{irrad} - J_{\varepsilon T} \tag{28}$$

Equation (28) shows that emissivity observability is governed by the balance between irradiance curvature and emissivity-temperature coupling. Adaptive dt-pair selection directly influences this balance by increasing temporal separation between t_1 and t_2, thereby enhancing irradiance contrast while enforcing a quasi-steady apparent surface temperature. This increases the irradiance curvature term and suppresses the relative influence of emissivity-temperature coupling.

3.4.3 Sensitivity analysis of the retrieved surface temperature

The retrieved surface temperature T_s depends on emissivity ε, upwelling longwave irradiance L, and downwelling longwave irradiance l. The total differential of T_s may be written as:

$$\delta T_s = \frac{\partial T_s}{\partial \varepsilon}\delta\varepsilon + \frac{\partial T_s}{\partial L_i}\delta L_i + \frac{\partial T_s}{\partial l_i}\delta l_i \tag{29}$$

The partial derivatives are evaluated at the converged Newton solution. Equation (29) reveals two distinct pathways: emissivity-driven sensitivity and irradiance-driven sensitivity.

The emissivity dependence enters exclusively through the temperature correction term ΔT. Differentiating Eq. (4) with respect to emissivity yields:

$$\frac{\partial T_s}{\partial \varepsilon} = -\frac{1}{8\sigma^{1/4}} \sum_{i=1}^{2}\left(\frac{L_i - l_i}{\varepsilon^2}\right)\left(\frac{L_i - l_i}{\varepsilon} + l_i\right)^{-3/4} \tag{30}$$

Equation (30) highlights several key properties. First, the ε^{-2} dependence produces strong nonlinear amplification as emissivity approaches unity, explaining why even small emissivity errors can generate large surface temperature perturbations over high emissivity surfaces. Second, the numerator $L_i - l_i$ represents the net surface radiant contrast; when this contrast is weak, such as under humid conditions, emissivity-driven sensitivity increases. Third, because $\delta\varepsilon$ itself is controlled by the Jacobian strength of the emissivity inversion, emissivity-driven temperature sensitivity directly inherits the conditioning of the emissivity retrieval. Poor emissivity observability therefore translates into unstable temperature estimates. Emissivity-driven sensitivity dominates when emissivity is weakly constrained, downwelling irradiance is large, irradiance contrast is small, and adaptive dt-pair selection is not applied.

https://doi.org/10.5194/egusphere-2026-858
Preprint. Discussion started: 2 April 2026

Irradiance-driven sensitivity arises from both terms in Eq. (29). Differentiation of the governing equation with respect to upwelling irradiance gives:

$$\frac{\partial T_s}{\partial L_i} = \frac{1}{8\sigma^{1/4}}\left[(L_i)^{-3/4} - \left(\frac{L_i - l_i}{\varepsilon} + l_i\right)^{-3/4}\right], \tag{31}$$

where the first term represents the direct Planck sensitivity of the apparent surface temperature and the second term accounts for emissivity correction. Their difference reflects how emissivity modifies the irradiance response. Differentiation with respect to downwelling irradiance yields:

$$\frac{\partial T_s}{\partial l_i} = -\frac{1}{8\sigma^{1/4}}\left(\frac{L_i - l_i}{\varepsilon} + l_i\right)^{-3/4}\left(1 - \frac{1}{\varepsilon}\right) \tag{32}$$

In this case sensitivity vanishes as $\varepsilon \to 1$. Downwelling irradiance affects T_s primarily over low-emissivity surfaces. This term is always negative, indicating that increased atmospheric emission reduces retrieved surface temperature. In typical environmental conditions, broadband longwave irradiances are large ($\approx$300-400 Wm^{-2}). The $L^{-3/4}$ scaling inherent in the model implies that sensitivity increases at lower irradiance levels, night-time and winter conditions tend to be more irradiance-sensitive than warmer daytime periods.

Combing all the terms we get the full sensitivity structure of T_s:

$$\delta T_s = \frac{\partial T_s}{\partial \varepsilon}\delta\varepsilon + \sum_{i=1}^{2}\left(\frac{\partial T_s}{\partial L_i}\delta L_i + \frac{\partial T_s}{\partial l_i}\delta l_i\right) \tag{33}$$

Adaptive dt-pair selection improves T_s stability since it improves emissivity observability, reduces $\delta\varepsilon$ and directly suppresses emissivity-driven sensitivity. Thus, improved T_s stability arises from conditioning, not from smoothing or noise suppression. The sensitivity of the retrieved surface temperature is governed by the balance between emissivity-driven and irradiance-driven pathways. Improving emissivity observability through adaptive time-pair selection reduces temperature sensitivity without modifying the underlying irradiance physics.

3.5 Uncertainty propagation analysis

Broadband longwave irradiances are measured using calibrated pyrgeometers. While per-sample numerical uncertainties are not always explicitly reported, instrument accuracy is inferred from calibration traceability and standard performance assessments documented for high-quality radiometric networks. For the purpose of quantifying the final uncertainty scale, the irradiance measurement uncertainty (σ_L) is set to a representative value consistent with the instrument performance standards established (Augustine et al., 2000):

$$\sigma_L = 2.0\,W\,m^{-2} = \text{Constant} \tag{34}$$

https://doi.org/10.5194/egusphere-2026-858
Preprint. Discussion started: 2 April 2026

This value σ_L serves as the input measurement uncertainty benchmark for this dataset. Unlike the simplified formulation often adopted in previous studies, irradiance errors in measurements are not strictly independent. Shared calibration constants, common atmospheric forcing and short-term drift introduce correlation both within channels (between L_1 and L_2, between l_1 and l_2) and across channels (between upwelling and downwelling irradiance). In this section two complementary uncertainty propagation approaches are examined: independent error propagation and correlated error propagation. Both formulations are implemented analytically and evaluated numerically using the same emissivity model. The independent case provides a diagnostic lower bound that isolates fundamental sensitivity pathways under idealized noise conditions, while the correlated case incorporates physically realistic covariance arising from shared calibration, atmospheric coherence, and cross channel coupling in longwave irradiance measurements.

3.5.1 Uncertainty propagation of the initial (linearized) emissivity

For reference, a lower-bound estimate of uncertainty is obtained by assuming that all measured components (L_1, l_1, L_2, l_2) are statistically independent and share a common instrument uncertainty $\sigma_{L_i} = \sigma_{l_i} = \sigma_L$. Under this assumption, first-order uncertainty propagation yields:

$$\sigma_{\varepsilon_0,ind} = \sqrt{\sum_{i=1}^{4}\left(\frac{\partial \varepsilon_0}{\partial x_i}\sigma_L\right)^2}, \qquad x_i \in \{L_1, l_1, L_2, l_2\} \tag{35}$$

The formulation in Eq. (35) represents a useful diagnostic baseline but neglects physically realistic covariance effects. It is appropriate when: instrument noise dominates, calibration errors are independent and atmospheric and surface effects do not induce cross-channel coupling.

Irradiance errors may be correlated due to: shared calibration constants, common atmospheric conditions and instrument drift. A more physically consistent uncertainty estimate is obtained by accounting explicitly for correlations among the irradiance measurements. Let the gradient of the linearized emissivity with respect to the irradiance vector $X = [L_1, l_1, L_2, l_2]^T$ be denoted by:

$$\nabla \varepsilon_0 = \begin{bmatrix} \partial \varepsilon_0 / \partial L_1 \\ \partial \varepsilon_0 / \partial l_1 \\ \partial \varepsilon_0 / \partial L_2 \\ \partial \varepsilon_0 / \partial l_2 \end{bmatrix}$$

The emissivity uncertainty is then expressed compactly as:

$$\sigma_{\varepsilon_0,corr} = \sqrt{\nabla \varepsilon_0^T \, \Sigma_L \, \nabla \varepsilon_0}, \tag{36}$$

where Σ_L is the irradiance covariance matrix. In practice, the covariance matrix is parameterized as:

https://doi.org/10.5194/egusphere-2026-858
Preprint. Discussion started: 2 April 2026

$$\Sigma_L = \sigma_L^2 \begin{bmatrix} 1 & \rho_c & \rho_L & \rho_c \\ \rho_c & 1 & \rho_c & \rho_l \\ \rho_L & \rho_c & 1 & \rho_c \\ \rho_c & \rho_l & \rho_c & 1 \end{bmatrix}, \tag{37}$$

where:

ρ_L is the correlation between upwelling irradiances (L_1, L_2),

ρ_l is the correlation between upwelling irradiances (l_1, l_2)

ρ_c is the cross-channel correlation between upwelling and downwelling irradiances.

This formulation naturally captures shared calibration effects, atmospheric coherence, and instrument drift.

3.5.2 Uncertainty propagation of Newton-retrieved emissivity

First, uncertainties in upwelling and downwelling longwave irradiances are assumed independent, Gaussian, and characterized by a common variance σ_L^2. For an emissivity ε defined implicitly by a nonlinear equation $f(\varepsilon; L) = 0$, first-order uncertainty propagation for implicit functions yields:

$$\sigma_\varepsilon^2 = \frac{\sigma_f^2}{\left|\partial f / \partial \varepsilon\right|^2}$$

where σ_f^2 is the variance of the residual function induced by irradiance uncertainty. The residual function f depends on irradiance differences and emissivity-corrected irradiance terms at both times. To first order, its variance is dominated by independent irradiance contributions:

$$\sigma_f^2 \approx 2\sigma_L^2, \tag{38}$$

with higher-order terms involving emissivity-temperature coupling contributing additional but bounded variance for realistic irradiance values. Consequently, σ_f^2 remains finite and directly controlled by instrument uncertainty. The uncertainty of the Newton-retrieved emissivity, under the independent structure, becomes:

$$\sigma_{\varepsilon,ind} = \frac{\sqrt{2}\sigma_L}{\left|\partial f / \partial \varepsilon\right|} \tag{39}$$

where $\partial f / \partial \varepsilon$ is the Jacobian evaluated at the Newton solution. This expression highlights the central role of the Jacobian: emissivity uncertainty is inversely proportional to local irradiance curvature.

Second, to incorporate correlated irradiance errors, the residual variance is generalized to:

$$\sigma_f^2 = W^T \Sigma_L W, \tag{40}$$

https://doi.org/10.5194/egusphere-2026-858
Preprint. Discussion started: 2 April 2026

where W is the sensitivity vector of the residual with respect to the irradiance inputs. For the two-time formulation used here, the dominant contribution arises from the upwelling irradiance difference, yielding:

$$W = [1,0,1,0]^T$$

The correlated Newton emissivity uncertainty therefore becomes:

$$\sigma_{\varepsilon,corr} = \frac{\sqrt{W^T \Sigma_L \nabla W}}{|\partial f / \partial \varepsilon|} \quad (41)$$

This formulation reduces to Eq. (39) when all correlations vanish, but more generally yields realistic uncertainty estimates when irradiance measurements are correlated.

Unlike the linearized emissivity, the Newton-retrieved emissivity uncertainty remains structurally bounded whenever the inversion is observable. As irradiance contrast weakens, the Jacobian decreases smoothly, leading to controlled and diagnostically meaningful increase in uncertainty rather than catastrophic divergence. Adaptive temporal pairing directly strengthens the Jacobian by enhancing irradiance contrast while preserving quasi-steady surface conditions, thereby suppressing uncertainty amplification.

This distinction explains the contrasting behavior observed in Figure 7: the linearized uncertainty exhibits non-physical spikes, while the Newton uncertainty remains well-behaved and interpretable across all cases. The covariance based formulation reinforces this interpretation by ensuring that uncertainty estimates reflect both instrument characteristics and the physical coupling structure of the inversion.

3.5.3 Uncertainty decomposition and interpretation for the surface temperature

This section analyzes the uncertainty structure of the retrieved surface temperature to identify the physical and numerical mechanisms that govern retrieval reliability beyond aggregate accuracy metrics. Because surface temperature uncertainty arises from multiple interacting pathways, including irradiance measurement noise, emissivity-temperature coupling, and inversion conditioning, explicit uncertainty decomposition is required to interpret observed errors and diagnose stability. Uncertainty is therefore examined under both independent error and correlated error assumptions. Considering both formulations is essential for distinguishing structural properties of the retrieval from artifacts of simplifying assumptions and for demonstrating that the bounded uncertainty behavior of the Newton-based frameworks persists under realistic error conditions.

Using first-order Taylor expansion, the variance of the corrected surface temperature under independent errors is expressed as:

$$\sigma^2_{T_s,ind} = \left(\frac{\partial T_s}{\partial \varepsilon}\right)^2 \sigma^2_{\varepsilon,ind} + \sum_i \left(\frac{\partial T_s}{\partial L_i}\right)^2 \sigma^2_L \quad (42)$$

https://doi.org/10.5194/egusphere-2026-858
Preprint. Discussion started: 2 April 2026

The summation index i spans all irradiance inputs $L_i \in \{L_1, L_2, l_1, l_2\}$. Equation (42) naturally separates the total temperature uncertainty into irradiance-driven and emissivity driven components.

The irradiance-driven component of surface temperature uncertainty arises from the explicit dependence of T_s on the measured irradiance fields. This contribution reflects the Planck law sensitivity of both the apparent surface temperature and the emissivity correction to perturbations in upwelling and downwelling longwave irradiance. Under the independent-error assumption, this component is obtained by summing the squared partial derivations of T_s with respect to each irradiance input, Eqs. (31) and (32), weighted by the common irradiance uncertainty, expressed as:

$$\sigma_{T_s,irrad,ind} = \sqrt{\sum_i \left(\frac{\partial T_s}{\partial L_i}\right)^2 \sigma_L^2} \tag{43}$$

Physically, this term represents the uncertainty that would remain even if emissivity were perfectly known. Its magnitude is governed by absolute irradiance levels and irradiance contrast and tends to increase under low irradiance conditions, such as nighttime or cold surface regimes. Importantly, this contribution is unaffected by the conditioning of the emissivity inversion and therefore provides a stable reference against which emissivity-driven effects can be evaluated.

The emissivity-driven component of the surface temperature uncertainty enters exclusively through the emissivity-induced correction term ΔT . As shown in Sect. 3.4.3, differentiation of the corrected temperature with respect to emissivity yields the sensitivity term in Eq. (30). Propagation of the independent emissivity uncertainty derived in Sect. 3.5.2, Eq. (39), then produces the emissivity-driven temperature uncertainty:

$$\sigma_{T_s,\varepsilon,ind} = \left|\frac{\partial T_s}{\partial \varepsilon}\right| \sigma_{\varepsilon,ind} \tag{44}$$

This component exhibits strong nonlinear amplification due to the explicit ε^{-2} dependence in the sensitivity expression. Consequently, even modest emissivity uncertainty can induce substantial temperature uncertainty when emissivity approaches unity or when surface-atmosphere irradiance contrast is weak. Because emissivity uncertainty itself is controlled by the Jacobian strength of the Newton inversion, this term directly reflects the numerical conditioning and physical observability of the emissivity retrieval.

Combining the irradiance-driven and emissivity-driven contributions yields the total independent-error surface temperature uncertainty:

$$\sigma_{T_s,ind} = \sqrt{\sigma_{T_s,\varepsilon,ind}^2 + \sigma_{T_s,irrad,ind}^2} \tag{45}$$

This decomposition makes explicit that surface temperature uncertainty is not governed solely by measurement noise magnitude, but by the interaction between irradiance sensitivity and emissivity observability. Under well-conditioned

https://doi.org/10.5194/egusphere-2026-858
Preprint. Discussion started: 2 April 2026

inversion, irradiance driven uncertainty typically dominates, while under weak irradiance contrast the emissivity-driven contribution becomes the principal source of amplification.

Adaptive temporal pairing reduces total temperature uncertainty in the independent-error framework indirectly, by improving emissivity observability and suppressing the propagated emissivity variance, while leaving the underlying irradiance measurement uncertainty unchanged. The independent error case therefore provides a physically interpretable lower bound on temperature uncertainty and establishes the reference against which the more realistic correlated-error formulation is evaluated. Because broadband longwave irradiance errors are not independent in practice, the following paragraphs extend the analysis to a correlated error formulation to assess how physically realistic covariance modifies the surface temperature uncertainty structure.

The independent-error formulation above provides a useful diagnostic lower bound on surface temperature uncertainty but neglects physically realistic correlations among broadband longwave irradiance measurements. Under correlated error, first-order uncertainty propagation yields a surface variance consisting of two additive contributions: a covariance-weighted irradiance term involving the full irradiance covariance matrix Σ_L, Eq. (37), and an emissivity-driven term obtained by propagating the correlated Newton emissivity, Eq. (41). This formulation generalizes the independent-error expression, Eq. (42) and reduces exactly to it when all off-diagonal covariance terms vanish, ensuring consistency.

The irradiance-driven component of surface temperature uncertainty under correlated errors arises from the explicit dependence of T_s on upwelling and downwelling irradiance. The required sensitivity terms are given by the partial derivatives derived in Sect. 3.4.3, Eqs. 31 and 32. Unlike the independent case, these sensitivities are now weighted by the full covariance structure rather than by a single variance. Formally, the correlated irradiance-driven temperature uncertainty is expressed as the quadratic form:

$$\sigma_{T_s,irrad,corr} = \sqrt{\nabla_L T_s^T \Sigma_L \nabla_L T_s}\ , \tag{46}$$

where $\nabla_L T_s$ denotes the gradient of the corrected surface temperature with respect to the irradiance vector with respect to the irradiance vector evaluated at the Newton solutions, and Σ_L is given by Eq. (37). Physically, this term captures how correlated perturbations in the irradiance fields propagate into surface temperature. Positive correlation between temporally adjacent upwelling irradiances reduces uncertainty in the mean apparent temperature, while cross-channel correlation modifies the effective contribution of the emissivity correction term. Depending on the sign and magnitude of the correlation coefficients, the irradiance-driven uncertainty may be modestly reduced or enhanced relative to the independent baseline. Importantly, this contribution remains bounded and smoothly varying, as it is governed by Planck-law sensitivity rather than inversion conditioning.

The emissivity-driven component of the surface temperature uncertainty under correlated errors arises from propagation of the correlated Newton emissivity uncertainty into the emissivity-induced temperature correction. The sensitivity of T_s with respect

https://doi.org/10.5194/egusphere-2026-858
Preprint. Discussion started: 2 April 2026

to emissivity is given by Eq. (30) and is unchanged from the independent-error formulation. Propagation of the correlated emissivity uncertainty derived in Sect. 3.5.2, Eq. (41), yields the emissivity-driven surface temperature uncertainty:

$$\sigma_{T_{s,\varepsilon,corr}} = \left|\frac{\partial T_s}{\partial \varepsilon}\right| \sigma_{\varepsilon,corr} \tag{47}$$

Because the Newton emissivity uncertainty is explicitly controlled by the Jacobian of the inversion, this term remains structurally bounded whenever emissivity is observable. As irradiance contrast weakens, the Jacobian decreases smoothly, leading to controlled and physically interpretable increase in emissivity-driven temperature uncertainty rather than the non-physical divergence associated with the linearized emissivity. Correlated irradiance errors therefore do not destabilize the temperature retrieval; instead, uncertainty growth remains governed by emissivity observability and inversion conditioning.

The total correlated-error surface temperature uncertainty is obtained by combing the irradiance-driven and emissivity-driven contributions:

$$\sigma_{T_s,corr} = \sqrt{\sigma^2_{T_{s,\varepsilon,corr}} + \sigma^2_{T_{s,irrad,corr}}} \tag{48}$$

This expression represents the physically realistic uncertainty of the corrected surface temperature in the presence of shared calibration effects, atmospheric coherence, and cross-channel coupling. In well-conditioned cases, the total uncertainty is dominated by the irradiance-driven component and closely resembles the independent-error baseline. In weakly conditioned cases, emissivity-driven uncertainty becomes dominant but remains bounded and diagnostically interpretable due to Jacobian control.

The correlated-error decomposition demonstrates that the bounded uncertainty behavior observed in the Newton-based surface temperature retrieval is not an artifact of the independent-error assumption. Instead, it reflects the intrinsic conditioning of the inversion and the explicit control of emissivity-driven amplification. By incorporating physically realistic covariance, the correlated formulation provides a robust and interpretable uncertainty estimate and confirms that adaptive temporal pairing improves temperature stability primarily by strengthening emissivity observability rather than by suppressing measurement noise.

3.6 Algorithmic integration and flow

The integration of the irradiance modeling, adaptive data selection and nonlinear inversion described in the preceding sections is summarized in the diagnostics framework show in Figure 1. This flowchart illustrates the logical progression from the initial selection of high-frequency temporal pairs to the final retrieval of the corrected surface temperature and uncertainty decomposition.

As shown in Figure 1, the retrieval is fundamentally governed by the Quasi-Steady Condition (Step), which serves as a physical and numerical filter. By enforcing a constraint on the change in apparent surface temperature between observation times (

https://doi.org/10.5194/egusphere-2026-858
Preprint. Discussion started: 2 April 2026

$\left|T_s^{'}(t_2) - T_s^{'}(t_1)\right| \le \Delta T_{\max}$), the algorithm adaptively adjusts the temporal separation to maximize irradiance contrast while preserving the physical assumption of emissivity invariance.

The transition from a linearized diagnostic estimate (Step 4) to the full Newton inversion (Step 5) ensures that the retrieval handles the nonlinear emissivity-temperature coupling rigorously. Furthermore, the framework incorporates post-hoc diagnostics and uncertainty decomposition (Steps 6 and 8), ensuring that every retrieved temperature is supported by an explicit assessment of inversion conditioning and parameter observability. This integrated approach allows the framework to remain structurally extensible to more complex radiative transfer scenarios while maintaining the diagnostic transparency required for high-precision ground-based validation.

https://doi.org/10.5194/egusphere-2026-858
Preprint. Discussion started: 2 April 2026

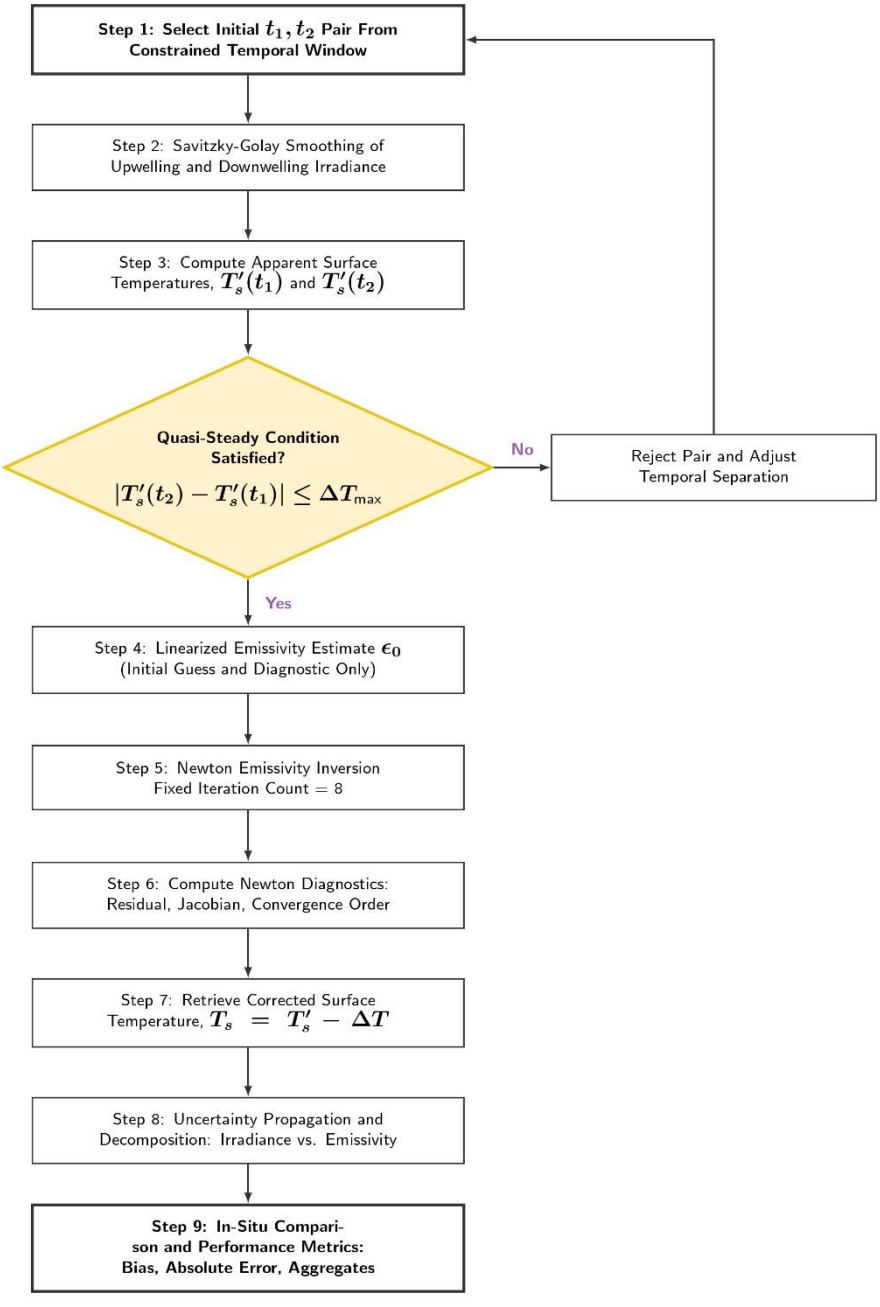

Figure 1. Flowchart of the diagnostic-driven retrieval framework for broadband land surface temperature (T_s) and surface emissivity (ε). The process integrates adaptive temporal pairing (t_1, t_2) constrained by the quasi-steady apparent surface temperature condition ($\left|T_s^{'}(t_2) - T_s^{'}(t_1)\right| \leq \Delta T_{max}^{'}$), followed by a nonlinear Newton-Raphson inversion with explicit convergence diagnostics. The framework concludes with formal uncertainty propagation and decomposition into irradiance-driven and emissivity-driven components to assess retrieval reliability prior to in-situ performance evaluation.

https://doi.org/10.5194/egusphere-2026-858
Preprint. Discussion started: 2 April 2026

4 Experimental setup and validation framework

This section describes the observational datasets, reference products, and contextual background used to evaluate the proposed broadband emissivity and surface temperature retrieval. It establishes the scope of the analysis, the basis for independent validation, and the limitations of commonly used approaches, thereby providing the necessary framework for interpreting the results presented in Sect. 5.

4.1 Data coverage and representativeness

The Surface Radiation Budget Network (SURFRAD) provides long-term, quality-controlled broadband irradiance measurements (Augustine et al., 2005). Four stations-Bondville (Illinois), Fort Peck (Montana), Goodwin Creek (Mississippi), and Sioux Falls (South Dakota) were used in this study. These stations operate in climatologically diverse regions and span a range of land cover types, surface conditions, and atmospheric regimes, including agricultural landscapes, grasslands, and mixed natural surfaces. As such, they provide a representative testbed for evaluating broadband emissivity observability and surface temperature retrieval under varying environmental conditions.

A total of thirty-nine data files acquired across different years, seasons, and atmospheric states were analyzed. The selected datasets encompass a wide range of surface temperatures, irradiance contrasts, and downwelling atmospheric contributions. This diversity allows the retrieval algorithm to be evaluated under both well-conditioned and weakly conditioned scenarios. All diagnostic, emissivity estimates (linearized and Newton-based), and corrected surface temperatures reported in subsequent sections are derived exclusively from this multi-site, multi-season dataset.

4.2 Reference emissivity and surface temperature for validation

The Surface Radiation Budget Network Independent reference values were required to evaluate the retrieved surface temperatures. For this purpose, broadband surface emissivity at each SURFRAD site was derived from satellite-based emissivity products. Specifically, emissivities from MODIS thermal infrared bands 31 and 32 were obtained from the 8-day MODIS land surface temperature product for dates nearest to the SURFRAD observations.

The narrowband emissivities were converted to broadband emissivity using the method proposed by (Wang et al., 2005; Wan, 2014). These broadband emissivities were then combined with SURFRAD upwelling longwave irradiance measurements and the Stefan-Boltzmann law to compute reference land surface temperatures. The resulting temperatures serve as external benchmark for evaluating the performance of the proposed retrieval algorithm. It is emphasized that satellite-derived emissivities and temperatures are used solely for validation purposes and are not used as inputs to the emissivity or surface temperature retrieval algorithm developed in this study.

https://doi.org/10.5194/egusphere-2026-858
Preprint. Discussion started: 2 April 2026

4.3 Context within existing SURFRAD-based approaches

Previous studies attempting to derive land surface temperatures from SURFRAD longwave irradiance measurements have often relied on satellite-derived narrowband emissivities, typically from MODIS thermal infrared bands (e.g., bands 29, 31, and 32). In many cases, emissivity values are obtained from global products such as MYD11C3, which provide monthly averages at a coarse spatial resolution (approximately 5 km).

Common practice involves selecting emissivity values from pixels nearest to the SURFRAD site location, applying quality masks, and averaging over a small spatial window (e.g., 3 x 3) pixels. While widely used, this approach introduces several sources of uncertainty, including: spatial mismatch between point-scale radiometric measurements and coarse satellite pixels; temporal mismatch between instantaneous in situ observations and multi-day or monthly satellite composites; spectral mismatch between narrowband satellite emissivities and broadband longwave irradiance exchange. The combined effect of these mismatches can significantly degrade the reliability of surface temperatures estimates derived from SURFARD irradiance measurements.

5 Results and discussion

This section presents a comprehensive evaluation of the proposed broadband emissivity and surface temperature retrieval algorithm, with emphasis placed on numerical and physical consistency rather than accuracy alone. Results are first examined in terms of Newton convergence characteristics, conditioning, and diagnostic indicators that govern the stability of the nonlinear inversion. The performance of the retrieved surface emissivity is then assessed, followed by validation of the corrected surface temperature against independent in-situ measurements. Finally, a detailed uncertainty analysis is presented, including explicit decomposition of surface temperature uncertainty into emissivity-driven and irradiance-driven components. Together, these results demonstrate that the reliability of the retrieval is governed by its numerical conditioning and diagnostic behavior, providing a transparent basis for interpreting accuracy and uncertainty across observational conditions.

5.1 Newton convergence behaviour and conditioning

The numerical stability and conditioning of the nonlinear emissivity inversion were first evaluated through a set of Newton convergence diagnostics derived directly from the iterative solution process. These diagnostics are independent of retrieval accuracy and instead assess whether the inversion is physically observable and numerically well posed under available radiometric constraints.

Figure 2 illustrates that residuals remain small across the full range of Jacobian values, confirming irradiance consistency. Importantly, no cases exhibit vanishing or near-singular Jacobians, indicating that the inversion avoids flat or ill-conditioned regimes. This behaviour confirms that the adaptive temporal pairing strategy successfully selects irradiance pairs that preserve physical observability while maintaining numerical stability.

https://doi.org/10.5194/egusphere-2026-858
Preprint. Discussion started: 2 April 2026

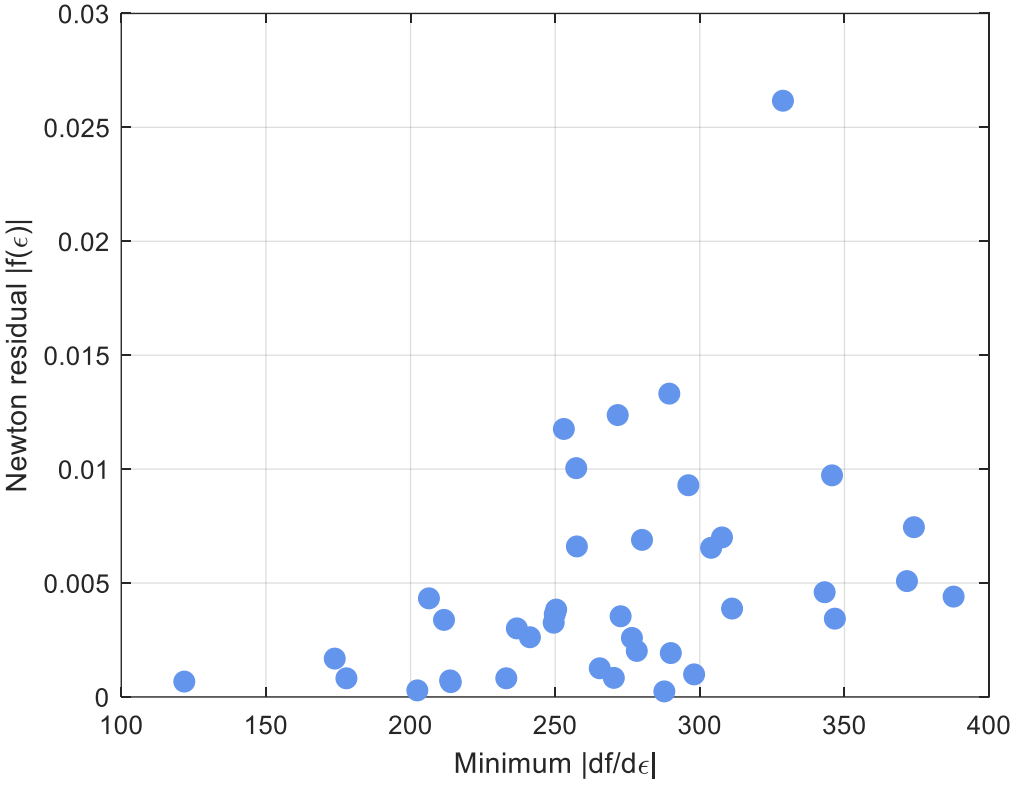

Figure 2. Relationship between the final Newton residual magnitude and the minimum absolute Jacobian value $|f(\varepsilon)|$ encountered during inversion. The absence of large residuals at small Jacobian magnitudes indicates that the emissivity inversion remains well conditioned and avoids singular or non-singular behavior across all cases.

The observed order of convergence p_k, computed from successive Newton iterates, is summarized in Figure 3 and reported quantitatively in Table 1. The distribution of p_k values is strongly concentrated near unity, with several cases marginally exceeding 0.9998 before rounding. When rounded to four decimal places, these values cluster tightly around one. While classical Newton theory predicts quadratic convergence in the asymptotic neighbourhood of an exact root, near-linear convergence is expected in the present application for several reasons: the inversion involves fractional-power irradiance terms, measurement noise is present in both upwelling and downwelling irradiances, and a fixed number of iterations is employed rather than asymptotic convergence to machine precision. Under these conditions, the observed convergence behaviour is stable, predictable, and fully consistent with theoretical expectations.

https://doi.org/10.5194/egusphere-2026-858
Preprint. Discussion started: 2 April 2026

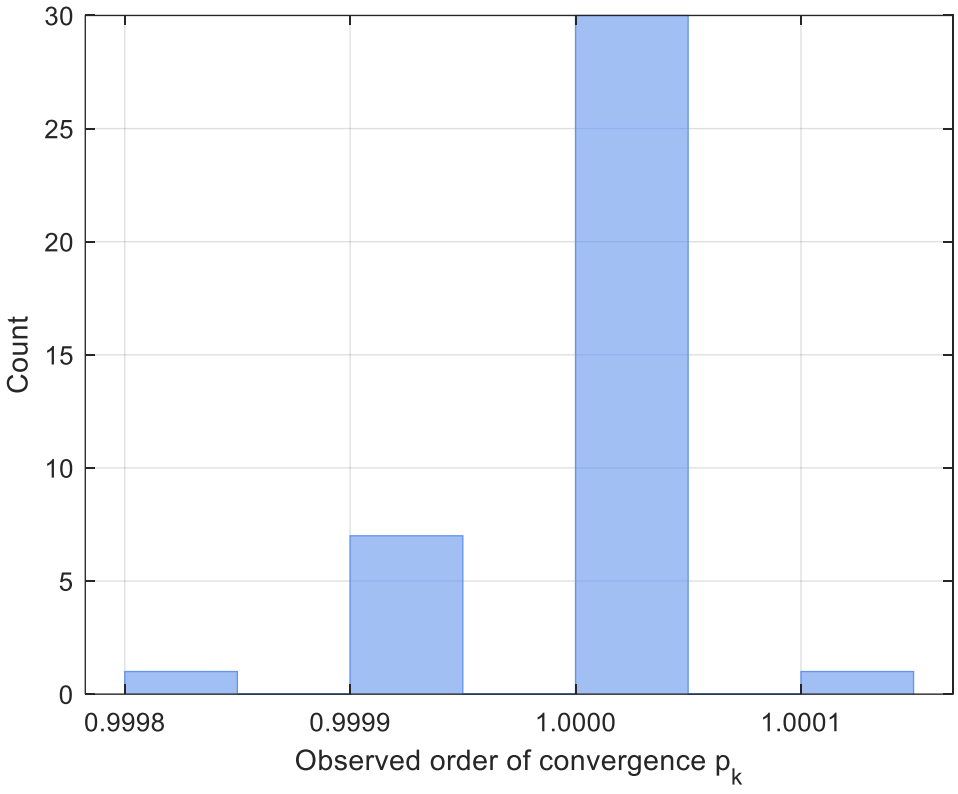

Figure 3. Distribution of the observed Newton convergence order p_k, rounded to four decimal places. Values cluster tightly around unity, with several cases approaching near-quadratic convergence before rounding, indicating stable and predictable nonlinear behavior under the fixed-iteration Newton scheme.

Crucially, no cases exhibit sub-linear convergence or erratic behavior, indicating that the Newton updates remain well directed throughout the inversion. The absence of convergence degradation further supports the conclusion that the emissivity inversion remains well conditioned across the full dataset. The numerical complexity of the retrieval involves two distinct iteration processes. The Newton-Raphson solver loop was executed with a fixed maximum count, $N_{Newton} \leq 8$ to allow for comprehensive diagnostic analysis. The adaptive temporal adjustment loop measures the effort required to select a numerically stable data pair. The count reported in Table 1 (labeled N_{adj}) and shown in Figure 4 quantifies this adaptive effort. For the vast majority of cases, N_{adj} is low, indicating that the initial temporal constraints already provided strong irradiance contrast. This distinction is critical: N_{adj} confirms data suitability while the analysis of the fixed N_{Newton} confirms solver stability. Because

https://doi.org/10.5194/egusphere-2026-858
Preprint. Discussion started: 2 April 2026

the observed convergence order p_k remains high (near 1.0) and stable (Figure 3), the fixed count $N_{Newton} \leq 8$ is demonstrated to be sufficient to achieve a solution precision constrained by the inherent irradiance uncertainty σ_L.

Table 1. Summary of the number of adaptive adjustments, minimum Jacobian magnitude, residual magnitude, and observed order of convergence for each dataset. These diagnostics quantify emissivity observability, numerical conditioning, and convergence behavior of the inversion and are used to distinguish well-conditioned and weakly conditioned retrievals.

Filename	dt1	dt2	N_{adj}	$\lvert f(\varepsilon)\rvert$	$\lvert\partial f/\partial\varepsilon\rvert$	p_k	Filename	dt1	dt2	N_{adj}	$\lvert f(\varepsilon)\rvert$	$\lvert\partial f/\partial\varepsilon\rvert$	p_k
bon13112	16.500	16.517	1	0.0010	298.0246	1.0000	fpk15081	17.767	17.783	1	0.0065	303.9075	1.0000
bon13119	16.617	16.633	1	0.0043	206.3541	1.0000	fpk15225	17.767	17.783	1	0.0044	387.7294	1.0000
bon13240	16.500	16.517	1	0.0008	177.8339	1.0000	fpk15232	17.867	17.883	1	0.0046	343.1558	1.0000
bon13247	16.617	16.633	1	0.0008	270.2683	1.0000	gwn14298	16.550	16.667	4	0.0003	202.3447	1.0000
bon13352	16.500	16.517	1	0.0007	121.7819	1.0000	gwn14307	16.433	16.583	5	0.0124	271.6169	0.9999
bon14042	16.600	16.617	1	0.0017	173.7947	1.0000	gwn14314	16.600	16.617	1	0.0013	265.4054	1.0000
bon14099	16.483	16.500	1	0.0039	311.1418	1.0000	gwn14355	16.500	16.517	1	0.0038	250.3373	1.0000
bon14106	16.583	16.600	1	0.0069	280.0147	0.9999	gwn15006	16.500	16.517	1	0.0034	211.5581	1.0000
bon14266	16.583	16.600	1	0.0026	241.2590	1.0000	gwn15038	16.500	16.517	1	0.0033	249.4866	1.0000
bon14298	16.583	16.600	1	0.0007	213.9134	1.0000	gwn15045	16.600	16.617	1	0.0133	289.4460	0.9999
bon15118	16.417	16.500	3	0.0262	328.7342	0.9998	gwn15125	16.583	16.600	1	0.0019	289.9700	1.0000
bon15214	16.450	16.467	1	0.0030	236.7523	1.0000	gwn15214	16.500	16.517	1	0.0007	213.6852	1.0000
bon15237	16.567	16.617	2	0.0066	257.4960	0.9999	gwn15237	16.467	16.750	9	0.0100	257.2731	0.9999
fpk13258	17.900	17.917	1	0.0035	272.6192	1.0000	sxf14292	17.183	17.200	1	0.0036	249.8544	1.0000
fpk13267	17.800	17.817	1	0.0002	287.7355	1.0000	sxf14308	17.133	17.250	4	0.0118	252.9918	0.9999
fpk13299	17.800	17.817	1	0.0008	233.0938	1.0000	sxf15087	17.167	17.183	1	0.0020	278.2063	1.0000
fpk14206	17.767	17.783	1	0.0070	307.6542	1.0000	sxf15103	17.167	17.183	1	0.0075	374.0069	1.0000
fpk14213	17.883	17.900	1	0.0034	346.6790	1.0000	sxf15112	16.933	17.217	9	0.0097	345.7011	1.0001
fpk14286	17.783	17.800	1	0.0093	296.0334	0.9999	sxf15119	17.167	17.183	1	0.0051	371.5949	1.0000
fpk14293	17.883	17.900	1	0.0026	276.5252	1.0000							

Figure 5 illustrates the relationship between the selected temporal separation and the retrieved Newton emissivity. The absence of any systematic dependence confirms that adaptive temporal pairing does not influence the emissivity solution itself, but instead functions as a neutral conditioning mechanism. This behavior is essential, as it demonstrates that convergence is achieved through appropriate data selection rather than through implicit modification of the inversion physics. The quasi-steady apparent surface temperature constraint therefore plays a critical dual role. Physically, it preserves the assumption that emissivity remains invariant over the selected time interval. Numerically, it prevents ill-posed inversions in which irradiance differences are dominated by surface temperature variability rather than emissivity sensitivity. Without this constraint, increasing temporal separation would introduce emissivity-temperature coupling that flattens the inversion surface and inflates uncertainty.

Convergence is therefore achieved through informed data selection rather than modification of the underlying physics. Consistent with the convergence diagnosis above, the results shown in Figure 5 demonstrate that this approach improves numerical conditioning while preserving physical neutrality, enabling stable emissivity retrieval across diverse surface and atmospheric conditions and providing a robust foundation for subsequent uncertainty analysis and surface temperature results.

https://doi.org/10.5194/egusphere-2026-858
Preprint. Discussion started: 2 April 2026

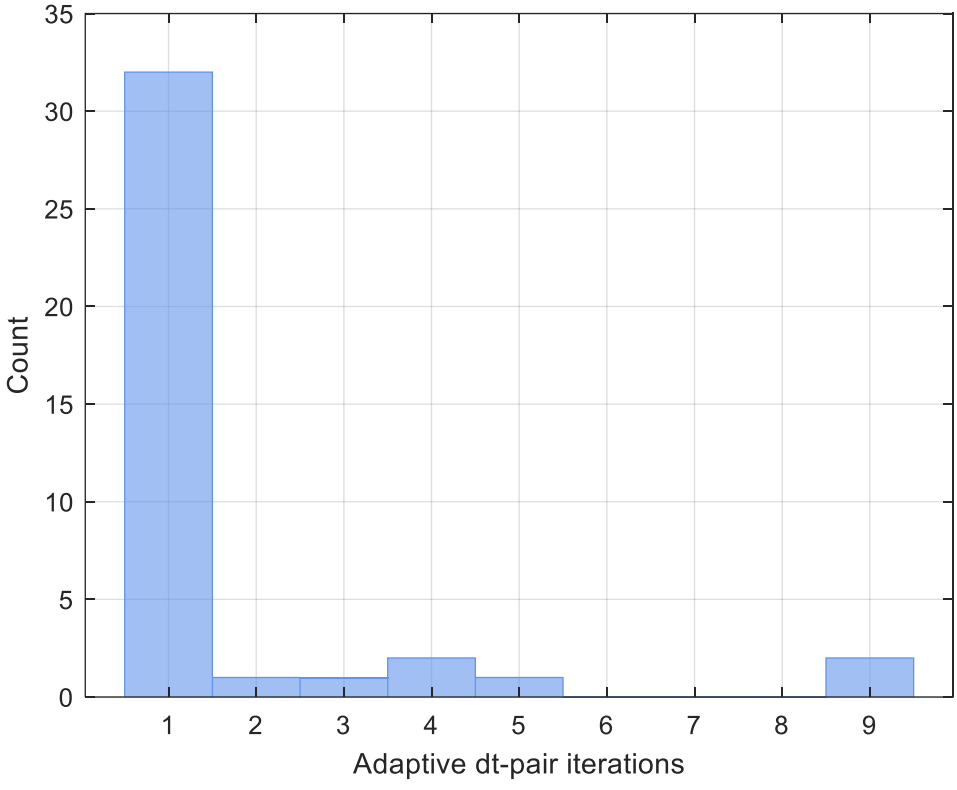

Figure 4. Distribution of adaptive dt-pair iteration counts required to obtain a physically admissible initial emissivity estimate. The low iteration counts observed for nearly all cases indicate that only minimal temporal adjustment is needed to satisfy the quasi-steady surface temperature constraint, confirming strong temporal observability.

Taken together, the residual magnitude, Jacobian strength, observed convergence order, and adaptive iteration counts provide complementary evidence that the Newton emissivity inversion is numerically stable, well-conditioned, and converges in a physically meaningful manner across diverse surface and atmospheric conditions. These diagnostics demonstrate that convergence arises from genuine irradiance information content rather than numerical artifact, establishing a robust foundation for interpreting the emissivity and surface temperature retrieval results presented in subsequent sections.

https://doi.org/10.5194/egusphere-2026-858
Preprint. Discussion started: 2 April 2026

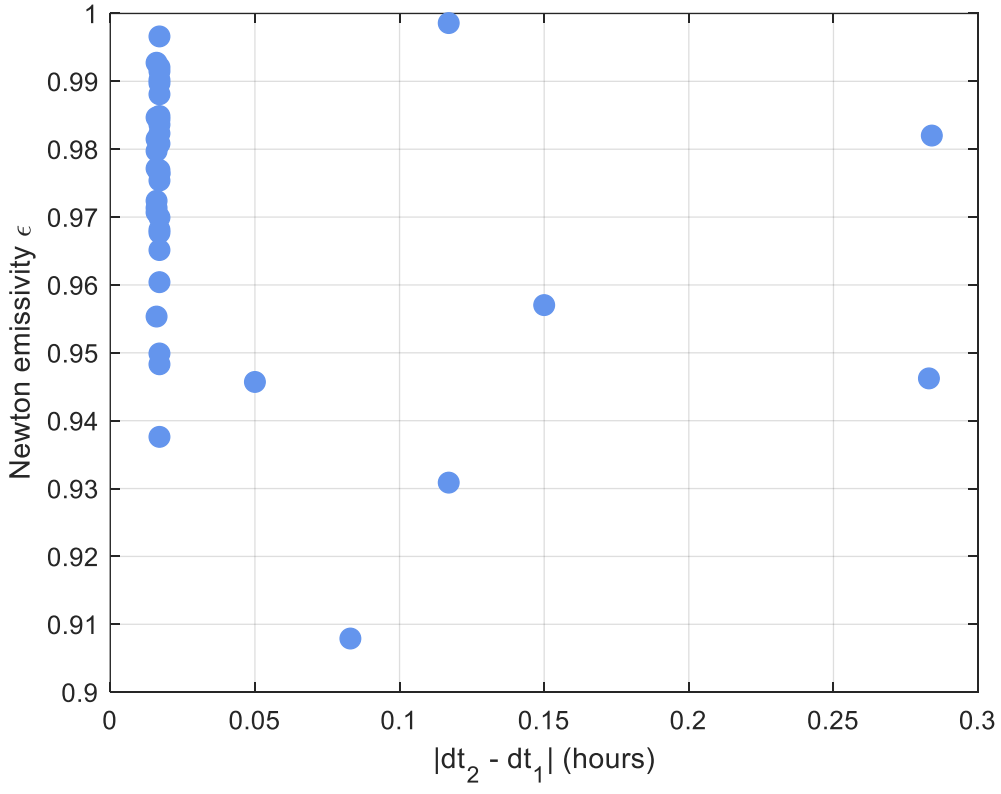

Figure 5. Relationship between the selected time separation $\Delta t = dt_2 - dt_1$ and the retrieved Newton emissivity. The adaptive dt-pair selection adjusts temporal spacing only as needed to maintain quasi-steady apparent surface temperature, improving numerical conditioning without altering the underlying irradiance model.

5.2 Emissivity retrieval results

This section evaluates the broadband emissivity retrieval performance, emphasizing the critical distinction between numerical magnitude and retrieval stability. Figure 6 compares the emissivity values obtained from the Newton inversion against those derived from the linearized approximation. While both approaches yield estimates of comparable magnitude, indicating that the linearized formulation provides a mathematically consistent starting point, this numerical agreement masks fundamental differences in the quality and robustness of the solutions.

The primary finding is that the reliability of the retrieved emissivity is not governed by its value, but by the conditioning of the framework used to find it. As established in the sensitivity analysis (Sect. 3.4.1), the linearized estimate is a first-order diagnostic that is highly susceptible to extreme uncertainty amplification under weak temporal contrast. In contrast, the Newton-based solution maintains its physical integrity across the entire dataset. The stability of the Newton inversion, enabled y explicit Jacobian control, ensures that the retrieval remains bounded even in low signal-to-noise ratio environments where

https://doi.org/10.5194/egusphere-2026-858
Preprint. Discussion started: 2 April 2026

the linearized model begins to exhibit non-physical behavior. Consequently, while the linearized estimate is retained as an efficient initialization tool, the Newton-based solution is identified as the only physically meaningful estimate capable of supporting high-precision surface temperature retrievals.

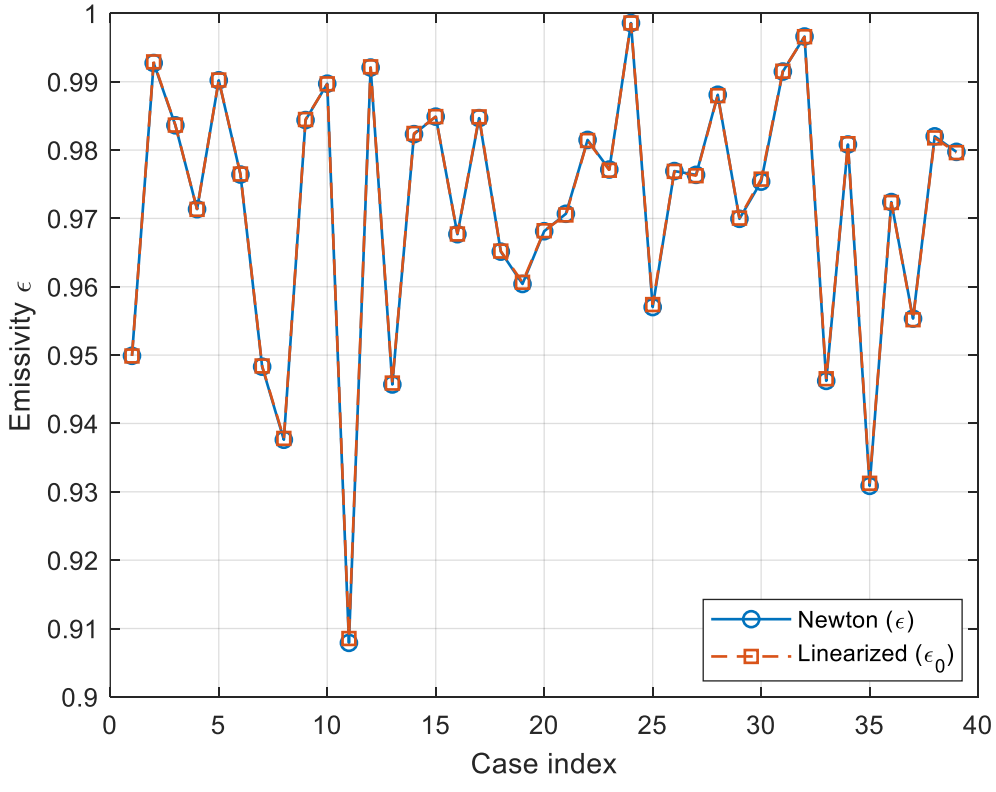

Figure 6. Comparison of emissivity obtained from the Newton inversion and the linearized approximation. While both approaches yield similar emissivity values, the linearized estimate is retained only as a diagnostic due to its strong conditioning dependence

The contrasting uncertainty behavior of the two formulations is illustrated in Figure 7, which compares correlated emissivity uncertainty for the Newton-retrieved emissivity (to panel) and the linearized emissivity (bottom panel). Although the retrieved emissivity values are similar, the associated uncertainty differs markedly. The linearized emissivity uncertainty is substantially larger and more variable, requiring a separate scale for visualization. This behavior reflects the strong conditioning dependence inherent in the linearized formulation, where uncertainty amplification is dominated by weak temporal irradiance contrast and denominator sensitivity. In contrast, the Newton emissivity uncertainty remains bounded and smoothly varying across all cases, consistent with Jacobian-controlled uncertainty propagation. This result confirms that the Newton inversion suppresses non-physical amplification by explicitly accounting for emissivity-temperature coupling and local curvature of the irradiance balance equation.

https://doi.org/10.5194/egusphere-2026-858
Preprint. Discussion started: 2 April 2026

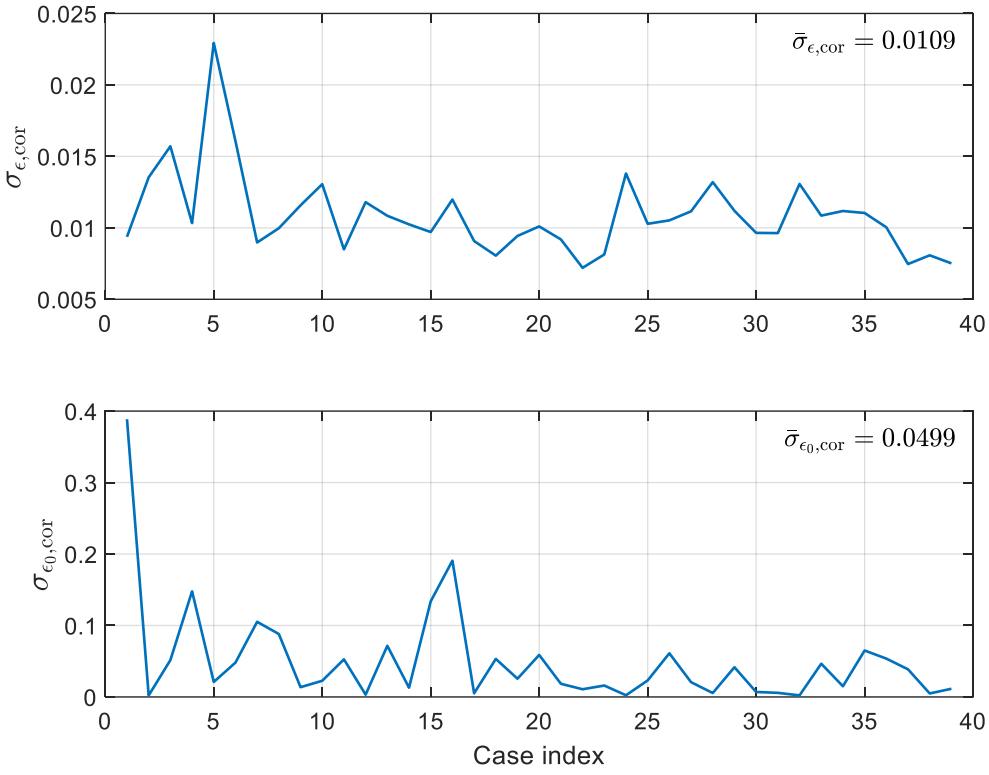

Figure 7. Comparison of correlated emissivity uncertainty components: Newton-retrieved emissivity uncertainty, (top), and linearized emissivity uncertainty (bottom), shown on separate scales. Although the retrieved emissivties are comparable, linearized is markedly larger and more variable, reflecting the stronger sensitivity of the linearized formulation to irradiance-based conditioning.

Figure 8 further examines emissivity uncertainty under independent and correlated irradiance error assumptions. Panel (a) shows Newton emissivity uncertainty assuming independent and correlated irradiance errors; when irradiance covariance is accounted for, the correlated-error formulation produces consistently larger uncertainty estimates. Panel (b) presents the same uncertainties on a case by case basis, revealing that correlation primarily introduces a consistent offset rather than altering the relative structure of uncertainty across cases. This behavior indicates that while irradiance covariance affects the absolute scale of emissivity uncertainty, it does not fundamentally change which cases are well or weakly conditioned. The persistence of bounded uncertainty under correlated errors confirms the stability of the Newton retrieval is not an artifact of idealized noise assumptions, but a consequence of improved emissivity observability.

https://doi.org/10.5194/egusphere-2026-858
Preprint. Discussion started: 2 April 2026

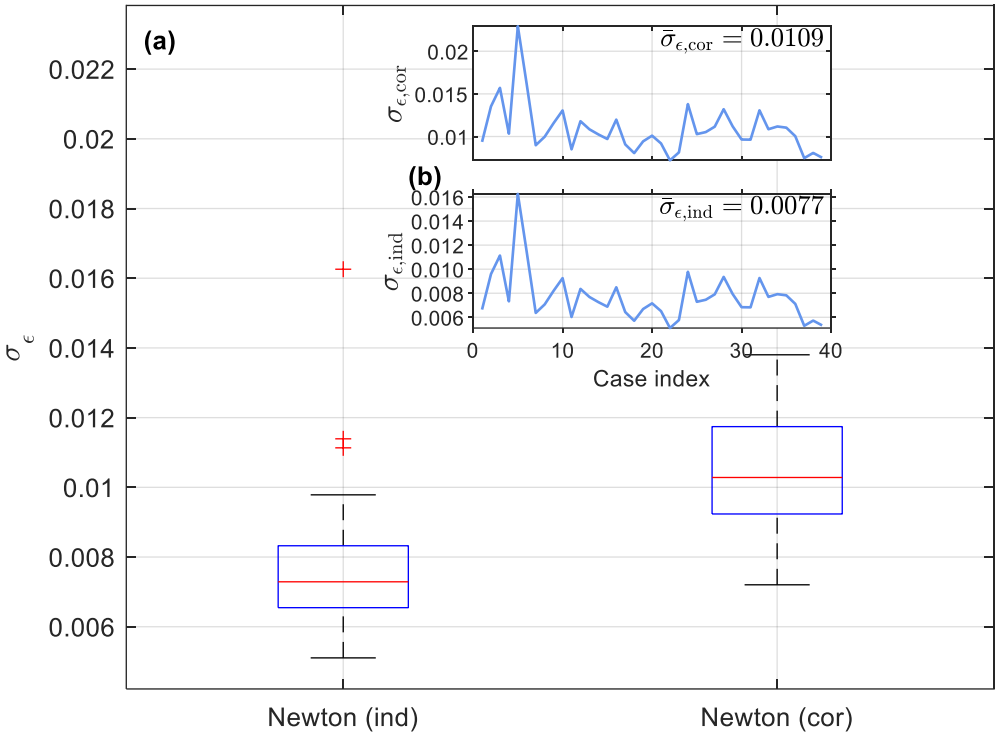

Figure 8. (a) Newton emissivity uncertainty under independent and correlated irradiance errors, with correlation increasing uncertainty magnitude; (b) corresponding case-wise uncertainties showing similar structure but systemic offset due to irradiance covariance.

Table 2 summarizes the broadband emissivity retrieval results and associated uncertainty estimates under both independent and correlated error assumptions. Newton and linearized emissivity values are reported alongside their corresponding uncertainty estimates, enabling direct comparison of retrieval magnitude and uncertainty behaviour. The table reinforces the graphical results: while emissivity values are broadly consistent between methods, the Newton-based uncertainty remains controlled under both error assumptions, whereas the linearized uncertainty exhibits strong sensitivity to conditioning. Together, these results demonstrate that reliable broadband emissivity retrieval can be achieved without externally prescribed emissivity products when numerical conditioning, convergence diagnostics, and uncertainty propagation are treated as integral components of the retrieval framework.

https://doi.org/10.5194/egusphere-2026-858
Preprint. Discussion started: 2 April 2026

Table 2. Broadband emissivity retrieval results and associated uncertainty estimates under independent and correlated error assumptions, showing Newton and linearized emissivity values together with emissivity uncertainties propagated from broadband longwave irradiance measurements.

Filename	ε	$\sigma_{\varepsilon,ind}$	$\sigma_{\varepsilon,corr}$	ε_0	$\sigma_{\varepsilon 0,ind}$	$\sigma_{\varepsilon 0,corr}$	Filename	ε	$\sigma_{\varepsilon,ind}$	$\sigma_{\varepsilon,corr}$	ε_0	$\sigma_{\varepsilon 0,ind}$	$\sigma_{\varepsilon 0,corr}$
bon13112	0.9499	0.0066	0.0094	0.9499	2.8736	0.3887	fpk15081	0.9707	0.0065	0.0092	0.9705	0.1306	0.0184
bon13119	0.9927	0.0096	0.0135	0.9929	0.0147	0.0021	fpk15225	0.9815	0.0051	0.0072	0.9814	0.0761	0.0108
bon13240	0.9836	0.0111	0.0157	0.9837	0.3956	0.0515	fpk15232	0.9772	0.0058	0.0081	0.9770	0.1135	0.0160
bon13247	0.9714	0.0073	0.0103	0.9713	1.0940	0.1478	gwn14298	0.9986	0.0098	0.0138	0.9986	0.0212	0.0023
bon13352	0.9902	0.0163	0.0229	0.9902	0.1515	0.0210	gwn14307	0.9570	0.0073	0.0103	0.9574	0.1720	0.0231
bon14042	0.9764	0.0114	0.0161	0.9765	0.3414	0.0481	gwn14314	0.9769	0.0075	0.0105	0.9769	0.4388	0.0611
bon14099	0.9483	0.0064	0.0090	0.9484	0.7721	0.1052	gwn14355	0.9764	0.0079	0.0112	0.9763	0.1475	0.0206
bon14106	0.9376	0.0071	0.0100	0.9378	0.6531	0.0880	gwn15006	0.9881	0.0094	0.0132	0.9880	0.0391	0.0055
bon14266	0.9844	0.0082	0.0116	0.9845	0.0977	0.0137	gwn15038	0.9699	0.0079	0.0112	0.9700	0.3044	0.0416
bon14298	0.9897	0.0093	0.0131	0.9897	0.1601	0.0226	gwn15045	0.9754	0.0068	0.0096	0.9758	0.0493	0.0070
bon15118	0.9079	0.0060	0.0085	0.9085	0.3960	0.0527	gwn15125	0.9915	0.0068	0.0096	0.9915	0.0414	0.0058
bon15214	0.9921	0.0084	0.0118	0.9922	0.0229	0.0032	gwn15214	0.9966	0.0093	0.0131	0.9966	0.0172	0.0022
bon15237	0.9457	0.0077	0.0108	0.9459	0.5456	0.0716	gwn15237	0.9462	0.0077	0.0109	0.9465	0.3563	0.0465
fpk13258	0.9823	0.0073	0.0102	0.9824	0.0918	0.0129	sxf14292	0.9808	0.0079	0.0112	0.9809	0.1074	0.0150
fpk13267	0.9849	0.0069	0.0097	0.9849	0.9496	0.1338	sxf14308	0.9309	0.0078	0.0110	0.9312	0.4899	0.0650
fpk13299	0.9677	0.0085	0.0120	0.9677	1.3967	0.1907	sxf15087	0.9724	0.0071	0.0100	0.9723	0.3798	0.0536
fpk14206	0.9847	0.0064	0.0091	0.9849	0.0363	0.0051	sxf15103	0.9553	0.0053	0.0075	0.9552	0.2748	0.0387
fpk14213	0.9651	0.0057	0.0081	0.9652	0.3901	0.0532	sxf15112	0.9820	0.0057	0.0081	0.9818	0.0393	0.0049
fpk14286	0.9604	0.0067	0.0094	0.9607	0.1862	0.0255	sxf15119	0.9797	0.0053	0.0075	0.9796	0.0844	0.0115
fpk14293	0.9681	0.0072	0.0094	0.9682	0.4296	0.0588							

5.2.1 Analysis of emissivity observability and inversion conditioning

The fundamental reliability of the broadband emissivity retrieval is governed by the interplay between the physical irradiance environment and the numerical stability of the Newton inversion. Figure 9 deconstructs this relationship by examining emissivity uncertainty and Jacobian conditioning as a function of irradiance contrast. Panel (a) illustrates the absolute uncertainty of the Newton-retrieved emissivity (σ_ε) across a spectrum of irradiance contrast conditions. A distinct power-law relationship is observed: as irradiance contrast approaches zero, representing a collapse of the signal-to-noise ratio where surface and atmospheric irradiances become nearly identical, the emissivity uncertainty increases from a baseline of approximately 0.006 to peak values exceeding 0.016. This trend aligns with theoretical expectations regarding the physical limit of emissivity observability; as the irradiance difference that labels the surface emissivity vanishes, the parameter becomes inherently more difficult to constrain.

This physical degradation is directly explained by the numerical conditioning shown in Panel (b). The minimum Jacobian magnitude ($\left|\partial f / \partial \varepsilon\right|$), which represents the sensitivity of the irradiance balance to changes in emissivity, exhibits a strong positive correlation with irradiance contrast. Jacobian values rise from near 150 at low contrast to approximately 400 in high-contrast regimes. Mathematically, the Jacobian defines the numerical grip the Newton solver has on the solution space; the

https://doi.org/10.5194/egusphere-2026-858
Preprint. Discussion started: 2 April 2026

lower Jacobian magnitudes observed at low contrast confirm that the inversion surface becomes locally flatter, thereby amplifying the propagation of measurement noise into the emissivity estimate. These observations confirm that the difficulty in retrieving emissivity at low contrast is not failure of the algorithm, but a fundamental property of the irradiance physics and inversion conditioning.

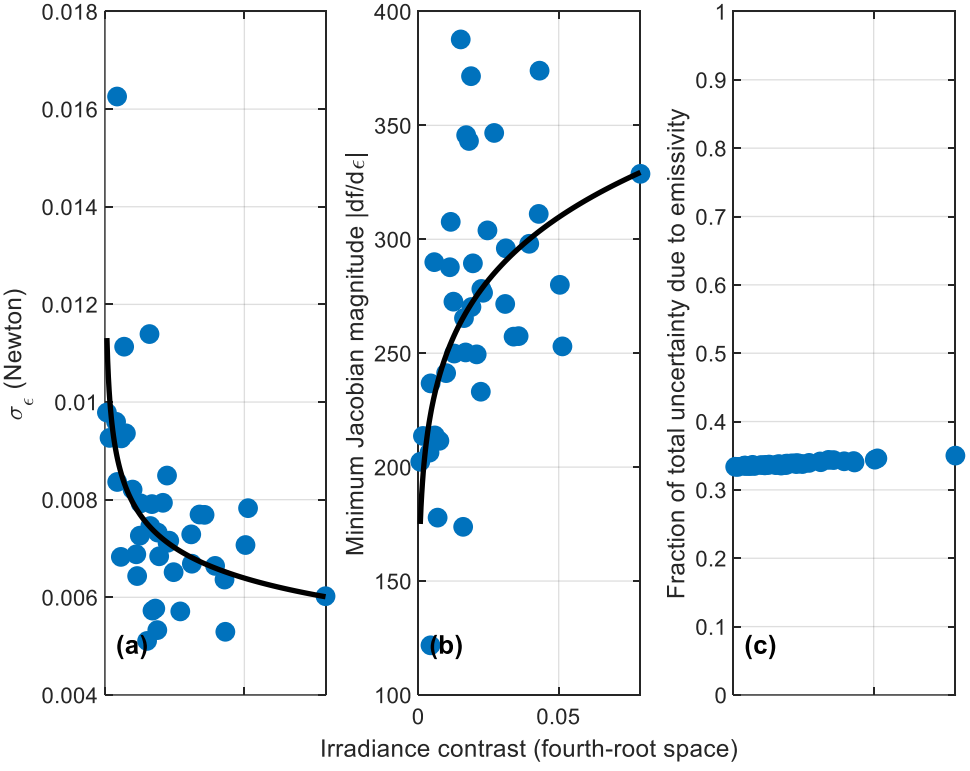

Figure 9. Determinants of the emissivity retrieval observability and conditioning. (a) Newton-based emissivity uncertainty (σ_ε) as a function of irradiance contrast; (b) minimum Jacobian magnitude ($|\partial f / \partial \varepsilon|$), illustrating the numerical strength of the inversion; and (c) the fractional contribution of emissivity to the total uncertainty budget. These panels illustrate that while low irradiance contrast degrades the Mathematical conditioning (Panel b) and increase parameter uncertainty (Panel a), the Newton framework prevents the instability from dominating the final temperature product (Panel c).

A critical finding of this analysis is the robustness of the temperature-emissivity coupling control, as is evidenced in Panel (c). Despite the three-fold increase in emissivity uncertainty and the significant weakening of the Jacobian at low contrast, the fraction of total temperature uncertainty due to emissivity remains remarkably stable at approximately 34%. This indicates that while emissivity itself becomes harder to retrieve under poor irradiance conditions, the Newton-based formulation

https://doi.org/10.5194/egusphere-2026-858
Preprint. Discussion started: 2 April 2026

successfully bounds its propagation into the final temperature product. The primary implication of these results is that the retrieval framework is diagnostically self-regulating. By explicitly accounting for the Jacobian strength, the method ensures the emissivity driven errors do not catastrophically amplify, allowing for reliable surface temperature estimation even when the signal-to-noise ratio for emissivity is significantly challenged. This diagnostic transparency ensures that the resulting precision is formally supported by the internal physics of the inversion rather than by external assumptions.

5.3 Surface temperature uncertainty analysis

To provide a rigorous evaluation of the Newton-based retrieval, the following sections deconstruct the surface temperature uncertainty (σ_{Ts}) into its fundamental physical and numerical drivers. This analysis moves beyond aggregate error metrics to examine the stability of the inversion under diverse conditions. Specifically, Sect. 5.3.1 investigates how the uncertainty budget responds to physical scene dynamics, focusing on the critical role of irradiance contrast and its impact on the signal-to-noise ratio. Subsequently, Sect. 5.3.2 evaluates the structural stability of the retrieval across discrete cases, quantifying how the transition from the idealized independent noise to realistic correlated error assumptions scales the absolute uncertainty without compromising the underlying sensitivity of the framework.

5.3.1 Irradiance contrast and SNR dynamics

The relationship between retrieval reliability and the physical state of the scene is best characterized by examining the dependence of surface temperature uncertainty (σ_{Ts}) on irradiance contrast. As shown in the scatter analysis of Figure 10, the Newton-based formulation exhibits a clear, physically consistent response to varying atmospheric and surface conditions. This relationship is essentially a function of the signal-to-noise ratio (SNR) inherent in the irradiance environment.

Panels (a) and (b) demonstrate that as irradiance contrast approaches zero, representing a regime where the signal-to-noise ratio is severely degraded because the surface and atmospheric signals become increasingly indistinguishable, and the absolute uncertainty in surface temperature increases. Crucially, this increase is not catastrophic; rather than exhibiting the numerical instability common in poorly conditioned inversions under low SNR conditions, the uncertainty remains bounded and diagnostically interpretable. This indicates that the Newton-based successfully preserves the inversion's physical meaning even when the observational signal is weak.

The fractional decomposition provided in Panel (c) reveals a fundamental characteristic of the uncertainty budget in relation to this signal-to-noise ratio. Irradiance-driven uncertainty consistently dominates the budget, accounting for approximately 65% to 67% of the total correlated error. This suggests that the primary limit on retrieval precision is the inherent measurement noise and its propagation through the Planck function, which sets the baseline for the signal-to-noise ratio.

Interestingly as irradiance contrast increases, effectively improving the signal-to-noise ratio, the irradiance driven fraction exhibits a marginal decline, while the emissivity-driven fraction shows a corresponding slight increase. This shift suggests that as the irradiance noise becomes a relatively less obstructive part of the signal, the accurate characterization of surface

https://doi.org/10.5194/egusphere-2026-858
Preprint. Discussion started: 2 April 2026

emissivity becomes a progressively more significant factor in achieving a high-precision temperature retrievals. In high SNR environments, the limiting factor shifts slightly from raw measurement noise toward the physical constraints of emissivity modeling.

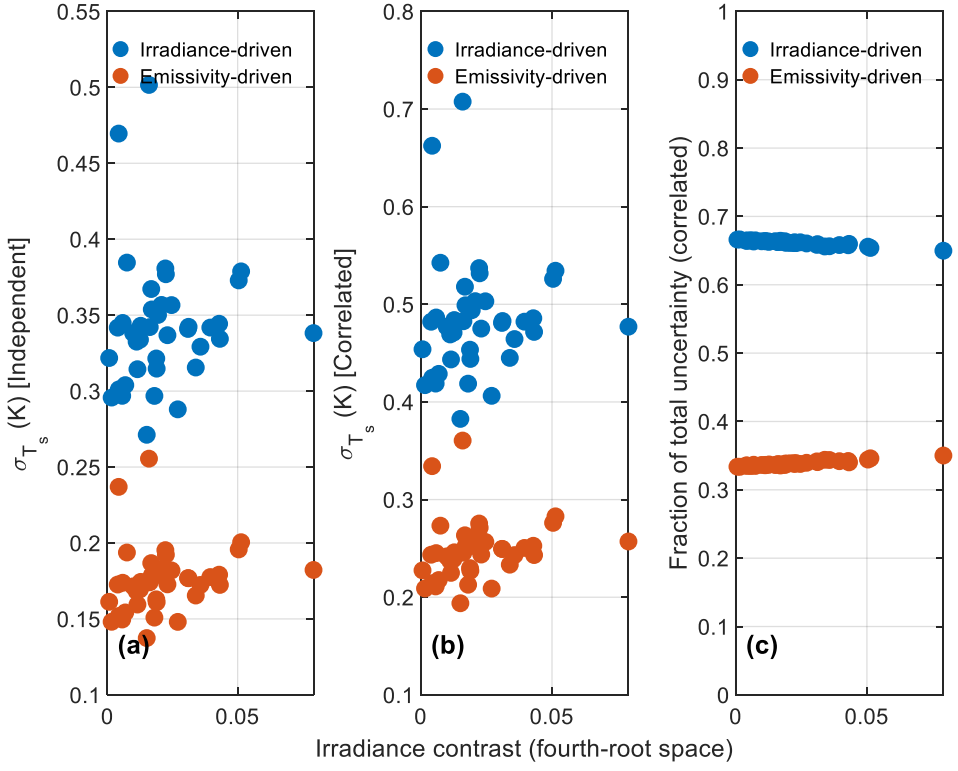

Figure 10. Surface temperature uncertainty components plotted as a function of irradiance contrast. Panel (a) shows the irradiance-driven and emissivity-driven surface temperature uncertainty under independent error assumptions; panel (b) shows the corresponding components under correlated irradiance error assumptions; panel (c) shows the fractional contribution of the irradiance-driven and emissivity-driven components to the total surface temperature uncertainty for the correlated case. Across all panels, uncertainty structure follows the same irradiance sensitivity patterns, while correlation primarily scales the uncertainty magnitude without altering the relative contribution of the two pathways.

5.3.2 Case-level stability and correlation scaling effects

While the previous analysis establishes how signal-to-noise ratio influences the error budget, Figure 11 examines the case-by-case structural stability of the uncertainty components across 39 discrete retrieval scenarios. This perspective allows for a direct comparison between idealized (independent) and realistic (correlated) irradiance errors assumptions.

https://doi.org/10.5194/egusphere-2026-858
Preprint. Discussion started: 2 April 2026

Under both assumptions, the total surface temperature uncertainty (σ_{Ts}^{tot}) and its constituents, irradiance-driven (σ_{Ts}^{irrad}) and emissivity-driven ($\sigma_{Ts}^{\varepsilon}$) components track one another with high structural fidelity. The peaks and valleys in the uncertainty profile occur at identical case indices across both panels, confirming that the underlying sensitivity is governed by the same Jacobian structure and irradiance sensitivities regardless of whether the error is modeled as independent or correlated.

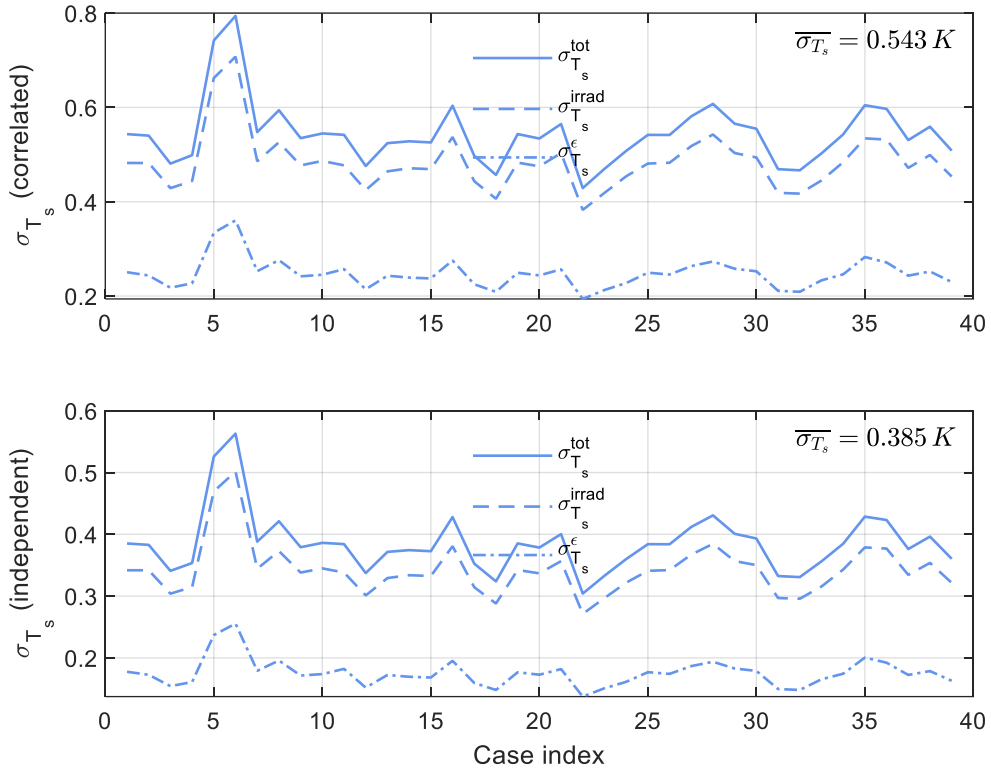

Figure 11. Decomposition of total corrected surface temperature uncertainty into irradiance-driven and emissivity-driven components for correlated (top) and independent (bottom) error assumptions. All components share similar structure because they depend on the same irradiance sensitivities, while correlation effects act primarily as scaling factors that shift uncertainty magnitude. Irradiance-driven uncertainty dominates, with emissivity-driven contributions remaining suppressed under Newton inversion.

The primary distinction between the two formulations is a systematic shift in magnitude that directly impacts the effective signal-to-noise ratio of the retrieval. The transition from independent to correlated error assumptions elevates the mean surface temperature uncertainty from $\overline{\sigma_{Ts}} = 0.385\,\mathrm{K}$ to $\overline{\sigma_{Ts}} = 0.543\,\mathrm{K}$. This 41% increase in the mean error highlights the importance of accounting for covariance effects; ignoring these correlations would result in an overestimation of the signal to noise ratio and an overly optimistic view of the retrieval precision. Importantly, even with the inclusion of correlated errors, the emissivity-

https://doi.org/10.5194/egusphere-2026-858
Preprint. Discussion started: 2 April 2026

driven component ($\sigma_{Ts}^{\varepsilon}$) remains consistently suppressed relative to the irradiance-driven component (σ_{Ts}^{irrad}). This confirms that the adaptive conditioning within the Newton framework effectively regulates the emissivity-temperature coupling, ensuring that the retrieval remains stable even when the signal-to-noise ratio is challenged. The result is a robust retrieval system where the error budget is predictably scaled by measurement covariance without altering the fundamental physical pathways through which uncertainty propagates. This diagnostic transparency ensures that the resulting sub-kelvin error statistics are formally supported by the internal physics of the inversion.

Table 3 reports the irradiance-driven and emissivity-driven components of surface temperature uncertainty under independent and correlated error assumptions, consistent with decomposition shown in Figure 11. These results indicate that the bounded surface temperature uncertainty of the Newton-based retrieval reflects intrinsic inversion conditioning and controlled emissivity-temperature coupling, rather than artifacts of idealized error assumptions or post-hoc noise suppression.

Table 3. Surface temperature uncertainty components under independent and correlated error assumptions. Irradiance-driven and emissivity-driven contributions to surface temperature uncertainty for the Newton-based retrieval, illustrating their relative importance under stable inversion conditions.

Filename	$\sigma_{T_s,\ ind}$ (K)	$\sigma_{T_{s,irrad},\ ind}$ (K)	$\sigma_{T_{s,\varepsilon},\ ind}$ (K)	$\sigma_{T_s,\ corr}$ (K)	$\sigma_{T_{s,irrad},\ corr}$ (K)	$\sigma_{T_{s,\varepsilon},\ corr}$ (K)	Filename	$\sigma_{T_s,\ ind}$ (K)	$\sigma_{T_{s,irrad},\ ind}$ (K)	$\sigma_{T_{s,\varepsilon},\ ind}$ (K)	$\sigma_{T_s,\ corr}$ (K)	$\sigma_{T_{s,irrad},\ corr}$ (K)	$\sigma_{T_{s,\varepsilon},\ corr}$ (K)
bon13112	0.3852	0.3418	0.1776	0.5434	0.4822	0.2505	fpk15081	0.4004	0.3566	0.1819	0.5648	0.5031	0.2567
bon13119	0.3829	0.3418	0.1726	0.5402	0.4821	0.2435	fpk15225	0.3041	0.2712	0.1374	0.4289	0.3826	0.1938
bon13240	0.3408	0.3039	0.1543	0.4808	0.4288	0.2176	fpk15232	0.3330	0.2968	0.1509	0.4697	0.4187	0.2128
bon13247	0.3536	0.3148	0.1610	0.4988	0.4440	0.2271	gwn14298	0.3599	0.3218	0.1613	0.5078	0.4539	0.2275
bon13352	0.5259	0.4695	0.2369	0.7419	0.6624	0.3342	gwn14307	0.3841	0.3409	0.1769	0.5418	0.4809	0.2495
bon14042	0.5629	0.5016	0.2555	0.7941	0.7076	0.3605	gwn14314	0.3839	0.3421	0.1741	0.5415	0.4827	0.2456
bon14099	0.3881	0.3443	0.1791	0.5475	0.4857	0.2527	gwn14355	0.4120	0.3672	0.1867	0.5811	0.5180	0.2634
bon14106	0.4212	0.3729	0.1958	0.5941	0.5260	0.2762	gwn15006	0.4306	0.3846	0.1937	0.6075	0.5426	0.2733
bon14266	0.3791	0.3381	0.1714	0.5348	0.4770	0.2418	gwn15038	0.4009	0.3567	0.1828	0.5655	0.5032	0.2579
bon14298	0.3862	0.3449	0.1738	0.5448	0.4865	0.2452	gwn15045	0.3932	0.3501	0.1790	0.5547	0.4939	0.2525
bon15118	0.3842	0.3382	0.1822	0.5419	0.4771	0.2571	gwn15125	0.3325	0.2969	0.1496	0.4690	0.4188	0.2111
bon15214	0.3373	0.3011	0.1519	0.4758	0.4248	0.2143	gwn15214	0.3308	0.2957	0.1481	0.4666	0.4172	0.2089
bon15237	0.3716	0.3292	0.1724	0.5242	0.4644	0.2432	gwn15237	0.3563	0.3155	0.1654	0.5026	0.4451	0.2333
fpk13258	0.3744	0.3339	0.1695	0.5282	0.4710	0.2391	sxf14292	0.3848	0.3430	0.1744	0.5428	0.4839	0.2460
fpk13267	0.3727	0.3325	0.1682	0.5257	0.4691	0.2373	sxf14308	0.4286	0.3788	0.2005	0.6046	0.5344	0.2829
fpk13299	0.4279	0.3808	0.1953	0.6037	0.5371	0.2755	sxf15087	0.4231	0.3769	0.1922	0.5969	0.5317	0.2712
fpk14206	0.3525	0.3144	0.1595	0.4973	0.4435	0.2250	sxf15103	0.3762	0.3344	0.1724	0.5307	0.4717	0.2432
fpk14213	0.3238	0.2880	0.1481	0.4568	0.4063	0.2089	sxf15112	0.3963	0.3538	0.1787	0.5591	0.4990	0.2521
fpk14286	0.3853	0.3423	0.1768	0.5435	0.4829	0.2494	sxf15119	0.3604	0.3215	0.1629	0.5084	0.4535	0.2298
fpk14293	0.3785	0.3368	0.1728	0.5340	0.4751	0.2437							

5.4 Surface temperature validation

This section evaluates the performance of the retrieved surface temperature against independent in-situ measurements to assess the physical realism and stability of the proposed retrieval framework. Validation is performed across a broad range of surface types, seasons, and atmospheric conditions, providing a stringent test of the combined emissivity-temperature inversion under both favorable and weakly conditioned irradiance regimes. The validation dataset used here was independently confirmed to

https://doi.org/10.5194/egusphere-2026-858
Preprint. Discussion started: 2 April 2026

be consistent with surface temperature values reported for the same SURFRAD stations and comparable atmospheric conditions (Zhang et al., 2016), ensuring that the present validation does not rely on unreferenced or duplicated benchmark data.

Figure 12 compares retrieved surface temperature against independent in-situ reference measurements for all cases. The close clustering of points around the one-to-one line indicates strong agreement between retrieved and measured temperature across the full dynamic range. The reported coefficient of determination (R^2=0.998) and root mean square error (RMSE=0.54), demonstrates that the retrieval achieves consistent accuracy without evidence of systematic bias. Importantly, deviations from the one-to-one line remain symmetric, indicating that residual errors are primarily random rather than structurally induced by the inversion.

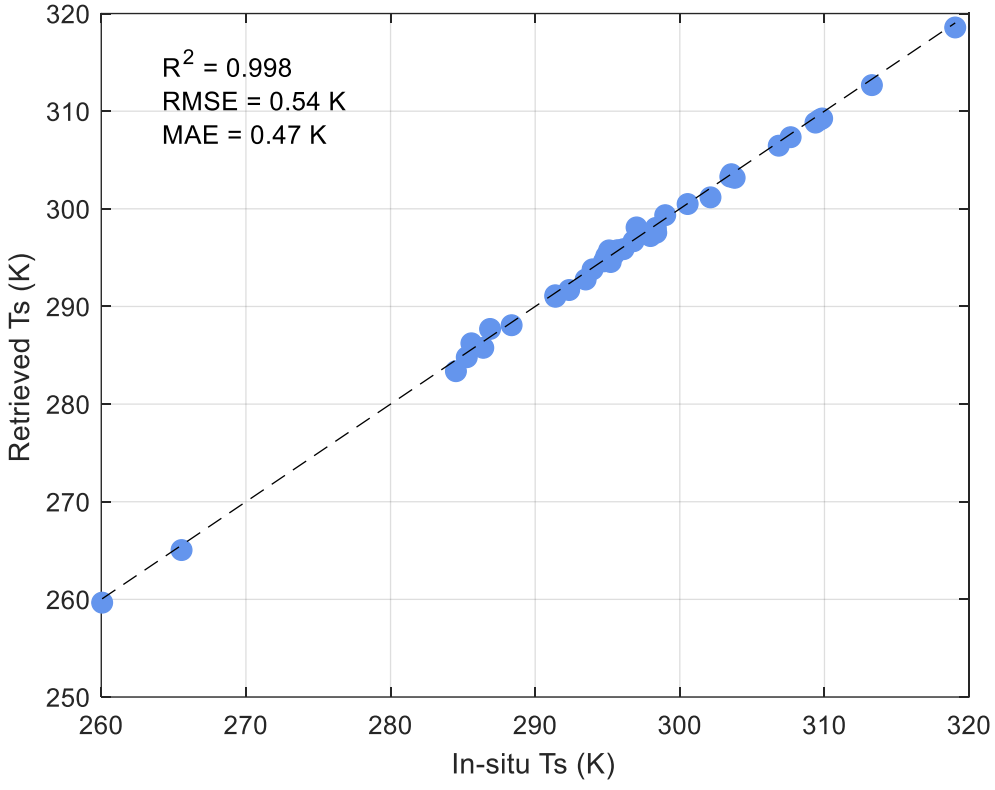

Figure 12. Comparison of retrieved surface temperature against independent in-situ measurements across all sites and seasons. The one-to-one reference line, along with reported R^2 and RMSE, indicates strong agreement and absence of systematic bias.

Table 4 summarizes validation statistics for both the Newton-based and linearized surface temperature retrievals relative to independent in-situ measurements, including retrieved temperature, bias, and absolute error. Across all cases, both approaches yield very similar mean bias and mean absolute error, indicating comparable average temperature accuracy. The distinction

https://doi.org/10.5194/egusphere-2026-858
Preprint. Discussion started: 2 April 2026

between the two methods is not in mean error magnitude, but in their numerical behaviour: the Newton-based retrieval maintains stable and bounded error characteristics across sites and atmospheric conditions, whereas the linearized formulation is more sensitive to irradiance conditioning. Overall, the close agreement with in-situ observations and consistency with formal uncertainty propagation demonstrate that reliable surface temperature retrieval can be achieved directly from broadband longwave irradiance measurements within the proposed diagnostic-driven framework.

Table 4. Validation statistics for Newton and linearized retrieved surface temperatures relative to in-situ measurements. Retrieved surface temperatures, bias and absolute error demonstrate improved and consistent performance of the Newton-bases retrieval across diverse sites and atmospheric conditions.

Filename	T_s (Newton)	T_s (In-situ)	T_s (Bias, Newton)	T_s (Abs-Error, Newton)	T_s (Bias, Linear)	T_s (Abs-Error, Linear)	Filename	T_s (Newton)	T_s (In-situ)	T_s (Bias, Newton)	T_s (Abs-Error, Newton)	T_s (Bias, Linear)	T_s (Abs-Error, Linear)
bon13112	295.7604	295.6900	0.0704	0.0704	0.0712	0.0712	fpk15081	291.1462	291.3900	-0.2438	0.2438	-0.2390	0.2390
bon13119	294.6245	294.7600	-0.1355	0.1355	-0.1385	0.1385	fpk15225	318.5723	319.0400	-0.4677	0.4677	-0.4653	0.4653
bon13240	306.4646	306.8400	-0.3754	0.3754	-0.3759	0.3759	fpk15232	309.2514	309.8400	-0.5886	0.5886	-0.5858	0.5858
bon13247	303.2988	303.4900	-0.1912	0.1912	-0.1907	0.1907	gwn14298	300.4909	300.5400	-0.0491	0.0491	-0.0493	0.0493
bon13352	265.0509	265.5500	-0.4991	0.4991	-0.4997	0.4997	gwn14307	295.7414	295.1100	0.6314	0.6314	0.6226	0.6226
bon14042	259.6644	260.0600	-0.3956	0.3956	-0.3973	0.3973	gwn14314	294.9164	295.1700	-0.2536	0.2536	-0.2527	0.2527
bon14099	295.1537	294.9100	0.2437	0.2437	0.2409	0.2409	gwn14355	288.0796	288.3700	-0.2904	0.2904	-0.2875	0.2875
bon14106	287.6966	286.8800	0.8166	0.8166	0.8112	0.8112	gwn15006	283.3725	284.5200	-1.1475	1.1475	-1.1448	1.1448
bon14266	295.8685	296.1100	-0.2415	0.2415	-0.2433	0.2433	gwn15038	290.9921	291.4000	-0.4079	0.4079	-0.4103	0.4103
bon14298	293.8016	293.9700	-0.1684	0.1684	-0.1679	0.1679	gwn15045	292.7617	293.4900	-0.7283	0.7283	-0.7379	0.7379
bon15118	298.0947	297.0100	1.0847	1.0847	1.0655	1.0655	gwn15125	308.8303	309.3800	-0.5497	0.5497	-0.5509	0.5509
bon15214	307.3362	307.6600	-0.3238	0.3238	-0.3257	0.3257	gwn15214	309.0967	309.6500	-0.5533	0.5533	-0.5529	0.5529
bon15237	299.3493	298.9900	0.3593	0.3593	0.3547	0.3547	gwn15237	303.5449	303.5600	-0.0151	0.0151	-0.0218	0.0218
fpk13258	297.2095	297.9700	-0.7605	0.7605	-0.7629	0.7629	sxf14292	294.5529	295.2200	-0.6671	0.6671	-0.6697	0.6697
fpk13267	297.5579	298.3700	-0.8121	0.8121	-0.8123	0.8123	sxf14308	286.2263	285.5900	0.6363	0.6363	0.6267	0.6267
fpk13299	284.8025	285.2700	-0.4675	0.4675	-0.4682	0.4682	sxf15087	285.7641	286.4100	-0.6459	0.6459	-0.6443	0.6443
fpk14206	303.1760	303.7900	-0.6140	0.6140	-0.6185	0.6185	sxf15103	298.0424	298.3400	-0.2976	0.2976	-0.2924	0.2924
fpk14213	312.6677	313.2800	-0.6123	0.6123	-0.6144	0.6144	sxf15112	291.6829	292.3500	-0.6671	0.6671	-0.6600	0.6600
fpk14286	295.3482	295.4600	-0.1118	0.1118	-0.1185	0.1185	sxf15119	301.1747	302.1200	-0.9453	0.9453	-0.9420	0.9420
fpk14293	296.6826	296.8000	-0.1174	0.1174	-0.1192	0.1192							

5.5 Summary performance metrics

To provide a concise quantitative summary of retrieval performance, aggregate metrics were computed across all sites, seasons, and atmospheric conditions considered in this study. The retrieved surface temperature exhibits a small mean bias of -0.2693 K, indicating the absence of systemic over- or underestimation. The root mean square error (RMSE) is 0.5443 K, while the mean absolute error is 0.4663 K, demonstrating consistent performance across a wide range of irradiance and surface conditions.

These error magnitudes are closely aligned with the formally propagated surface temperature uncertainty. Under the independent-error assumption, the mean total uncertainty is 0.3853 K, while inclusion of irradiance covariance increases the mean total uncertainty to 0.5435 K. The close agreement between the observed validation error (RMSE=0.5443 K) and the

https://doi.org/10.5194/egusphere-2026-858
Preprint. Discussion started: 2 April 2026

correlated uncertainty estimate confirms internal consistency between diagnostic uncertainty propagation and external validation performance, indicating that residual errors are largely explained by measurement-driven uncertainty rather than numerical instability.

The emissivity retrieval exhibits similarly stable behavior. The mean Newton-retrieved emissivity uncertainty is 0.0077 under independent errors and 0.0109 when irradiance covariance is included, remaining well bounded across all cases. This result reinforces the conclusions of Sections 5.1-5.3: under well-conditioned Newton inversion, emissivity uncertainty remains physically interpretable and controlled by irradiance contrast and Jacobian strength. In contrast, the linearized emissivity, while often close in value, exhibits substantially larger and more variable uncertainty and is therefore retained strictly as a diagnostic indicator rather than a physically meaningful estimate.

Overall, these summary metrics confirm that the proposed retrieval framework achieves reliable surface temperature estimation not only in terms of accuracy, but also in terms of numerical stability, conditioning, and uncertainty control. The close correspondence between observed validation error and the correlated, irradiance-driven uncertainty demonstrates that surface temperature errors are consistent with expected measurement limitations and are not dominated by unsuppressed emissivity-driven amplification. This agreement between diagnostic uncertainty estimates and validation performance provides strong evidence for the physical reliability and robustness of the derived surface temperature and emissivity products.

6 Conclusions

This study presents a conditioning-controlled retrieval framework for estimating broadband surface emissivity and land surface temperature directly from paired ground-based upwelling and downwelling longwave irradiance measurements. Using high-temporal-resolution SURFRAD observations as a measurement testbed, the retrieval is formulated as a nonlinear inverse problem in which numerical conditioning, parameter observability, and uncertainty structure are treated as intrinsic components of the measurement interpretation rather than secondary numerical details. In this respect, the approach aligns explicitly with inverse-problem theory (Rodgers, 2000; Tarantola, 2005) by emphasizing diagnostic consistency, Jacobian-controlled stability, and physically interpretable uncertainty propagation in addition to conventional accuracy metrics.

A central result of this work is the demonstration that broadband emissivity and surface temperature retrieval are fundamentally governed by irradiance contrast and inversion conditioning. Although linearized emissivity formulations may yield values numerically close to nonlinear solutions, their associated uncertainty structure becomes ill-conditioned under common observational regimes characterized by strong atmospheric downwelling irradiance and weak temporal contrast. The divergence of linearized emissivity uncertainty is shown to be a structural consequence of the linear approximation when the signal-to-noise ratio of the irradiance contrast becomes insufficient to support stable inversion.

In contrast, the Newton-based formulation enforces the full nonlinear irradiance balance and explicitly accounts for emissivity–temperature coupling. Emissivity uncertainty is governed by the inversion Jacobian and therefore remains bounded whenever emissivity is observable. As irradiance contrast weakens, uncertainty increases smoothly and diagnostically rather than

https://doi.org/10.5194/egusphere-2026-858
Preprint. Discussion started: 2 April 2026

catastrophically, providing physically interpretable information regarding retrieval reliability. This bounded behavior confirms that inversion stability is controlled by conditioning diagnostics rather than by numerical artifacts.

The surface temperature retrieval benefits significantly from the robust characterization of emissivity within the Newton-based framework. By explicitly decomposing temperature uncertainty into emissivity-driven and irradiance-driven components, the analysis clarifies the physical pathways through which uncertainty propagates. Contrary to typical assumptions in low-signal regimes, irradiance-driven uncertainty remains the dominant contributor under weak irradiance contrast, reflecting the sensitivity of the retrieval to the signal-to-noise ratio. While emissivity-driven uncertainty remains a secondary component, its relative importance increases slightly as irradiance contrast improves. Adaptive temporal pairing enhances surface temperature precision indirectly by improving emissivity conditioning, thereby stabilizing the inversion without altering the baseline irradiance uncertainty. Validation against independent in-situ measurements confirms this consistency, with sub-Kelvin error statistics that align with the formally propagated, correlated uncertainty.

From Diagnostic Framework to Operational Efficiency: The selection of a fixed, maximum $N_{Newton} \leq 8$ for the iterative solver was a deliberate choice for this validation study, allowing for transparent diagnosis of the Jacobian and convergence order. For operational implementation, this is superseded by a dynamic stopping criterion: (1) Monitoring the Jacobian magnitude, to halt the retrieval if it approaches an ill-conditioned regime (typically $\partial f / \partial \varepsilon < 10^2$); and (2) terminating the Newton iteration when the change in emissivity $|\varepsilon_{k+1} - \varepsilon_k|$ is less than a tolerance defined by the formally propagated emissivity uncertainty σ_ε. This transition ensures the algorithm remains both scientifically transparent and computationally efficient.

Extensibility of the Framework: Although the current study's validation is rigorously constrained to surface-based observations where atmospheric transmittance and emission terms are limited to the downwelling path, the core of the proposed diagnostic framework is mathematically general. The fundamental methodology-Newton inversion, Jacobian based conditioning diagnostics, and uncertainty decomposition, can be directly applied to more complex radiative transfer problems, such as those encountered in satellite bases LST retrieval. Extending the framework only requires modifying the irradiance model (Equation 1) to incorporate the full atmospheric transmittance and upwelling emission terms, which introduce additional, but treatable, complexity into the Jacobian structure $\partial f / \partial \varepsilon$. The key finding, that LST retrieval reliability is governed by the Jacobian of the inversion, remains universally valid regardless of the specific radiative transfer terms included. Future work will focus on integrating a full radiative transfer model into the Jacobian, to demonstrate the framework's applicability to high-altitude or space radiometric networks.

By explicitly linking emissivity observability, numerical conditioning, adaptive temporal pairing, and formal uncertainty propagation, this study establishes a transparent and reproducible methodology for extracting physically reliable broadband surface temperature and emissivity estimates from ground-based longwave irradiance measurements. The framework complements existing validation efforts by embedding diagnostic conditioning control directly within the retrieval design, thereby strengthening the interpretability and physical reliability of measurement-based surface temperature estimation.

https://doi.org/10.5194/egusphere-2026-858
Preprint. Discussion started: 2 April 2026

Competing interests

The author declare no conflicts of interest.

Acknowledgements

The author gratefully acknowledge the U.S. Department of Energy Atmospheric Radiation Measurement (ARM) program for providing the Surface Radiation Network (SURFRAD) data used in this study. The high quality, long-term broadband irradiance measurements made available through SURFRAD were essential for the development and evaluation of the retrieval methodology presented in this work.

Financial support

This research received no external funding.

References

Aster, R. C., Borchers, B., and Thurber, C. H.: Parameter Estimation and Inverse Problems, 3rd ed., Elsevier Academic Press, Cambridge, MA, USA, 2019.

Augustine, J. A., DeLuisi, J. J., and Long, C. N.: SURFRAD—A national surface radiation budget network for atmospheric research, Bull. Am. Meteorol. Soc., 81, 2341–2357, https://doi.org/10.1175/1520-0477(2000)081<2341:SANSRB>2.3.CO;2, 2000.

Augustine, J. A., Hodges, G. B., Cornwall, C. R., Michalsky, J. J., and Medina, C. I.: An update on SURFRAD—The GCOS surface radiation budget network for the continental United States, J. Atmos. Ocean. Technol., 22, 1460–1472, https://doi.org/10.1175/JTECH1806.1, 2005.

Dash, P., Göttsche, F.-M., Olesen, F.-S., and Fischer, H.: Land surface temperature and emissivity estimation from passive sensor data: Theory and practice; current trends, Int. J. Remote Sens., 23, 2563–2594, https://doi.org/10.1080/01431160110115041, 2002.

Dennis, J. E. and Schnabel, R. B.: Numerical Methods for Unconstrained Optimization and Nonlinear Equations, Society for Industrial and Applied Mathematics, Philadelphia, PA, USA, 1996.

Gillespie, A. R., Rokugawa, S., Matsunaga, T., Cothern, J. S., Hook, S. J., and Kahle, A. B.: A temperature and emissivity separation algorithm for Advanced Spaceborne Thermal Emission and Reflection Radiometer (ASTER) images, IEEE Trans. Geosci. Remote Sens., 36, 1113–1126, https://doi.org/10.1109/36.700995, 1998.

https://doi.org/10.5194/egusphere-2026-858
Preprint. Discussion started: 2 April 2026

Hulley, G. C. and Hook, S. J.: Generating consistent land surface temperature and emissivity products between ASTER and MODIS data for Earth science research, IEEE Trans. Geosci. Remote Sens., 49, 1304–1315, https://doi.org/10.1109/TGRS.2010.2063034, 2011.

Li, S., Yu, Y., Sun, D., Tarpley, D., Zhan, X., and Chiu, L.: Evaluation of 10-year AQUA/MODIS land surface temperature with SURFRAD observations, Int. J. Remote Sens., 35, 830–856, https://doi.org/10.1080/01431161.2013.873149, 2014.

Li, Z.-L., Li, L., Tang, B.-H., and Cribb, M. C.: A review of methods for retrieving land surface emissivity from space, Remote Sens. Environ., 231, 111199, https://doi.org/10.1016/j.rse.2019.111199, 2019.

Li, Z.-L., Tang, B.-H., Wu, H., Ren, H., Yan, G., Wan, Z., Trigo, I. F., and Sobrino, J. A.: Satellite-derived land surface temperature: Current status and perspectives, Remote Sens. Environ., 131, 14–37, https://doi.org/10.1016/j.rse.2012.12.008, 2013.

Li, Z.-L., Wu, H., Duan, S.-B., Zhao, W., Ren, H., Liu, X., Leng, P., Tang, R., Ye, X., Zhu, J., Sun, Y., Si, M., Liu, M., Li, J., Zhang, X., Shang, G., Tang, B.-H., Yan, G., and Zhou, C.: Satellite remote sensing of global land surface temperature: Definition, methods, products, and applications, Rev. Geophys., 61, e2022RG000777, https://doi.org/10.1029/2022RG000777, 2023.

Menke, W.: Geophysical Data Analysis: Discrete Inverse Theory, 3rd ed., Academic Press, Burlington, MA, USA, 2012.

Nocedal, J. and Wright, S. J.: Numerical Optimization, Springer, New York, NY, USA, 2006.

Norman, J. M., Kustas, W. P., and Humes, K. S.: A two-source approach for estimating soil and vegetation energy fluxes from observations of directional radiometric surface temperature, Agric. For. Meteorol., 77, 263–293, https://doi.org/10.1016/0168-1923(95)02265-Y, 1995.

Ortega, J. M. and Rheinboldt, W. C.: Iterative Solution of Nonlinear Equations in Several Variables, Society for Industrial and Applied Mathematics, Philadelphia, PA, USA, https://doi.org/10.1137/1.9780898719468, 2000.

Rodgers, C. D.: Inverse Methods for Atmospheric Sounding: Theory and Practice, World Scientific, Singapore, https://doi.org/10.1142/3171, 2000.

Tarantola, A.: Inverse Problem Theory and Methods for Model Parameter Estimation, Society for Industrial and Applied Mathematics, Philadelphia, PA, USA, https://doi.org/10.1137/1.9780898717921, 2005.

Wan, Z.: New refinements and validation of the collection-6 MODIS land-surface temperature/emissivity product, Remote Sens. Environ., 140, 36–45, https://doi.org/10.1016/j.rse.2013.08.027, 2014.

Wang, M., Zhang, Z., Hu, T., and Liu, X.: A practical single-channel algorithm for land surface temperature retrieval: Application to Landsat series data, J. Geophys. Res. Atmos., 124, 299–316, https://doi.org/10.1029/2018JD029330, 2019.

Zhang, Z., He, G., Wang, M., Long, T., Wang, G., and Zhang, X.: Validation of the generalized single-channel algorithm using Landsat 8 imagery and SURFRAD ground measurements, Remote Sens. Lett., 7, 810–816, https://doi.org/10.1080/2150704X.2016.1190475, 2016.